Monthly Notices
of the
ROYAL ASTRONOMICAL SOCIETY

MNRAS **444,** 3015–3039 (2014) doi:10.1093/mnras/stu1642

Spitzer/Infrared Array Camera near-infrared features in the outer parts of S^{4}G galaxies

Seppo Laine,[1⋆] Johan H. Knapen,[2,3] Juan-Carlos Muñoz-Mateos,[4,5] Taehyun Kim,[4,5,6,7] Sébastien Comerón,[8,9] Marie Martig,[10] Benne W. Holwerda,[11] E. Athanassoula,[12] Albert Bosma,[12] Peter H. Johansson,[13] Santiago Erroz-Ferrer,[2,3] Dimitri A. Gadotti,[5] Armando Gil de Paz,[14] Joannah Hinz,[15] Jarkko Laine,[8,9] Eija Laurikainen,[8,9] Karín Menéndez-Delmestre,[16] Trisha Mizusawa,[4,17] Michael W. Regan,[18] Heikki Salo,[8] Kartik Sheth,[1,4,19] Mark Seibert,[7] Ronald J. Buta,[20] Mauricio Cisternas,[2,3] Bruce G. Elmegreen,[21] Debra M. Elmegreen,[22] Luis C. Ho,[7,23] Barry F. Madore[7] and Dennis Zaritsky[24]

Affiliations are listed at the end of the paper

Accepted 2014 August 11. Received 2014 August 6; in original form 2014 May 13

ABSTRACT

We present a catalogue and images of visually detected features, such as asymmetries, extensions, warps, shells, tidal tails, polar rings, and obvious signs of mergers or interactions, in the faint outer regions (at and outside of R_{25}) of nearby galaxies. This catalogue can be used in future quantitative studies that examine galaxy evolution due to internal and external factors. We are able to reliably detect outer region features down to a brightness level of 0.03 MJy sr^{-1} pixel^{-1} at 3.6 μm in the *Spitzer* Survey of Stellar Structure in Galaxies (S^{4}G). We also tabulate companion galaxies. We find asymmetries in the outer isophotes in 22 ± 1 per cent of the sample. The asymmetry fraction does not correlate with galaxy classification as an interacting galaxy or merger remnant, or with the presence of companions. We also compare the detected features to similar features in galaxies taken from cosmological zoom re-simulations. The simulated images have a higher fraction (33 per cent) of outer disc asymmetries, which may be due to selection effects and an uncertain star formation threshold in the models. The asymmetries may have either an internal (e.g. lopsidedness due to dark halo asymmetry) or external origin.

Key words: atlases – catalogues – galaxies: interactions – galaxies: peculiar – galaxies: structure – infrared: galaxies.

1 INTRODUCTION

Performing studies of the internal or external factors that cause galaxies to evolve is predicated on the availability of statistically significant numbers of target galaxies that exhibit resolvable, implicative signs of these processes. One way to do this is by observing a large sample of nearby galaxies and searching for faint features that exist at or outside their outer 'edges' (at or outside the 25 mag arcsec^{-2} *B*-band isophotes; 'R_{25}'). Such features may be a sign of past interactions and mergers that the targeted galaxy has undergone in its recent or even extended (billions of years) past (e.g. Vorontsov-Velyaminov 1959, 1977; Arp 1966; Toomre & Toomre 1972; Hibbard & Yun 1999; Hibbard et al. 2001). Gas accretion from the intragalactic medium, possibly from filaments, may be the cause for faint outer features such as warps and polar rings, in addition to asymmetry (e.g. Ostriker & Binney 1989; Bournaud & Combes 2003; Macció, Moore & Stadel 2006; Brook et al. 2008; Jog & Combes 2009). Internal causes for asymmetry include lopsidedness due to dark halo asymmetry (e.g. Jog & Combes 2009; Zaritsky et al. 2013). Therefore, statistics of the frequency of existence of these features around nearby galaxies will help us to assess the importance of the aforementioned processes on galaxy evolution.

The main approach to detecting faint features in the outer regions of galaxies is through visual classification (e.g. Sandage 2005, and references therein). One of the most well-known catalogues of unusual features in and around galaxies is 'Arp's Atlas of Peculiar Galaxies' (Arp 1966). Another fundamentally important visual classification of interacting and merging galaxies was made

⋆ E-mail: seppo@ipac.caltech.edu

by Toomre & Toomre (1972). Other more recent attempts to visually classify galaxy morphology include 'The de Vaucouleurs Atlas of Galaxies' (Buta, Corwin & Odewahn 2007) and 'Galaxy Morphology' (Buta 2013). The quantitative approach to detecting unusual galaxy features based on e.g. asymmetry, concentration, clumpiness, and the Gini inequality parameter (e.g. Abraham & Merrifield 2000; Bershady, Jangren & Conselice 2000; Abraham, van den Bergh & Nair 2003; Conselice 2003; Lotz, Primack & Madau 2004; Scarlata et al. 2007; Muñoz-Mateos et al. 2009; Holwerda et al. 2011, 2014; Huertas-Company et al. 2013) works better in regions of high signal-to-noise ratio (S/N), namely, in the inner regions of galaxies. Thus, these two approaches are often complementary, as the quantitative method will miss faint features at or outside the outer edges of galaxies, where the eye can pick up features (e.g. Adams et al. 2012; Hoyos et al. 2012) that can form the basis for future quantitative studies after much deeper, high S/N images are available. Indeed, when detecting features in the outermost regions of galaxies (or outside their continuous luminous bodies), such as outer disc asymmetries, warps, tidal features, etc., it can be argued that the human eye is still often the most effective tool for picking up faint patterns (although attention needs to be paid to erroneous identifications, such as faint residual images). False positive detections can be reduced to some degree by using more than one person to detect the features of any given galaxy. The effort to avoid false positive detections, although not in the context of faint outer features, has been taken to its extreme in the Galaxy Zoo project (www.galaxyzoo.org; Lintott et al. 2008, 2011), which allows anyone to go online and categorize a shown galaxy with references to a few illustrated morphological choices. An automated detection and classification of galaxy features with the help of neural networks has also been attempted (e.g. Storrie-Lombardi et al. 1992; Lahav 1995; Goderya & Lolling 2002; Ball et al. 2004, 2008; Fukugita et al. 2007; Shamir 2009; Cheng et al. 2011), but so far it has worked better in assigning galaxies into broad morphological classes based on inner large-scale features, rather than in detecting weak patterns outside the main bodies of galaxies. Because any remaining image artefacts are more prominent outside the main bodies of galaxies, any automatic feature detections there would likely have to be checked by eye, further reducing the usefulness of automatic detection methods outside R_{25}.

The visual detection of features at or outside the outer edges of galaxies may be used to obtain an estimate of the rate of current and recent interactions, the merger rate, the frequency and importance of external gas accretion from the intergalactic reservoir, the number of companion galaxies, statistics on the asymmetries of galactic haloes, and the disc structure overall. The intrinsic limitations in visual detections include naturally the depth and spatial resolution of the data, the flat-fielding accuracy, and the effects of interference from other perturbing astronomical or instrumental sources, such as scattered light from nearby bright stars and image artefacts, and the techniques used to look at the data (including the visual acuity of the person performing the detection, of course!). Recent work on detecting faint features outside the main galaxy discs include those by Martínez-Delgado et al. (2010), Tal et al. (2010), Adams et al. (2012), and Atkinson, Abraham & Ferguson (2013). On the other hand, a morphological classification of mostly bright inner features within the discs of an initial set of galaxies from the *Spitzer* Survey of Stellar Structure in Galaxies (S^{4}G; Sheth et al. 2010) was made by Buta et al. (2010), with classifications for the remaining galaxies in Buta et al. (2014). An attempt to classify tidal features in S^{4}G, including shells, was made by Kim et al. (2012). Other major attempts to visually detect inner features in fairly large samples of nearby galaxies include those by Fukugita et al. (2007) and Nair & Abraham (2010).

In future the number of suitably observed galaxies will increase to millions (e.g. with the Large Synoptic Survey Telescope, LSST), and it will not be feasible to perform human eye-based feature detection by experts in these new samples. Therefore, visual search for faint features in relatively large galaxy samples, consisting of thousands of galaxies, such as S^{4}G, will also form a good training basis for automated computer algorithms that recognize patterns and classify them in the future. We have selected the visual detection method in this work because we are just beginning to look for tidal and other types of outer features. Quantitative or automatic methods are already good in quantifying something that is known to exist in high S/N data, and will grow increasingly powerful in detecting faint features in images in the future (cf. Hales et al. 2012). Our current effort emphasizes the detection and discovery of subtle new features, possibly related to tidal interaction or accretion, which are best picked up by eye, but can perhaps be automatically detected with sophisticated codes in the future. Follow-up work may be able to quantify our new discoveries. In this paper we refer to already performed quantitative work that was based on the high S/N regions of the galaxies in the S^{4}G sample (Kim et al. 2012; Zaritsky et al. 2013; Holwerda et al. 2014), and therefore, inside R_{25}. The current paper thus complements the earlier work on S^{4}G and extends it farther out in radius, where it presents discoveries of faint features that should be quantified in the future when higher S/N observations are available. Ellipse fits to the *Spitzer*/Infrared Array Camera (IRAC) images and parameters derived from these fits are given in Muñoz-Mateos et al. (2014) and are available in the NASA/IPAC Infrared Science Archive (IRSA) at http://irsa.ipac.caltech.edu/data/SPITZER/S4G/. However, it should be noted that in the outermost galaxy regions that we are surveying in this paper, the ellipse fits are too uncertain to be trusted and some of the outer features cannot be approximated by ellipse fits at all, leaving the visual detection as the only viable way to find new faint features there.

S^{4}G consists of near-infrared (IR) images and thus has some unique advantages over conventional visual band images. First, the spectral energy distribution of late-type stars, including many luminous asymptotic giant branch stars, peaks in the near-IR, and may thus reveal features that are not clearly visible at shorter wavelengths. Second, in general, the dominant light in the near-IR is coming from older stars than the light at shorter wavelengths, thus revealing longer lived, major dynamical features, as opposed to recent bursts of star formation. Eskew, Zaritsky & Meidt (2012) and Meidt et al. (2012a,b) show that it is possible to separate the contributions from the various stellar components and measure the mass directly with the help of S^{4}G near-IR images. Therefore, the longer term time evolution of galaxies can be better studied. Third, the effects of cold dust that can block features from view are dramatically reduced in the near-IR. In our study, in which we look at features mostly outside the main galaxy bodies or at the edges of them, the effects of dust are generally thought to be less important than closer to the centre of galaxies, but some of the features that we classify, such as shells, polar rings, or even warps, may be blocked from view at least partially at visible light wavelengths. Additional benefits of S^{4}G, as explained in Section 2, are the uniformity and depth of the S^{4}G images across the sample and finally, the spatial coverage of the images, which around most sample galaxies extends to at least $1.5R_{25}$ in radius, making this sample amenable to morphological classification of faint features in the outer parts of galaxies.

2 SAMPLE AND DATA

The sample we used is the full S^{4}G sample (Sheth et al. 2010), consisting of 2352 galaxies (10 of the 2331 galaxies specified in Sheth et al. 2010 were not observed, mostly because they were close to a very bright star, and 31 galaxies were added) with systemic velocity $V_{\rm sys,radio} < 3000$ km s^{-1}, corresponding to a distance $d < 45$ Mpc for a *Planck*-mission-based Hubble constant (Ade et al. 2014) of 67 km s^{-1} Mpc^{-1} and a distance $d < 41$ Mpc for a Hubble constant of 71 km s^{-1} Mpc^{-1}, total corrected blue magnitude $m_{B\rm corr} < 15.5$, blue light isophotal angular diameter $D_{25} > 1.0$ arcmin, and a Galactic latitude $|b| > 30^\circ$ (Sheth et al. 2010). All the galaxies in this sample were imaged with the *Spitzer Space Telescope*'s IRAC (Fazio et al. 2004). We used the channel 1 (3.6 μm) mosaics made of eight 30-s frames per spatial position. The survey is described in detail in Sheth et al. (2010) which is the main reference for the S^{4}G sample and data. 597 galaxies in the sample already had observations in the *Spitzer* Heritage Archive, and almost all of them have a total frame time depth of at least 240 s (that of the new observations). The only exceptions are NGC 5457 (96 s), NGC 0470 and NGC 0474 (150 s), and NGC 5218, NGC 5216, and NGC 5576 (192 s). Several of the archival observations are from the *Spitzer* Infrared Nearby Galaxies Survey (SINGS; Kennicutt et al. 2003) and the Local Volume Legacy Survey (LVL; Dale et al. 2009) Legacy Projects that had a very similar mapping strategy to the S^{4}G observations.

We started with the basic calibrated data (BCDs) that are the fundamental IRAC pipeline-reduced images from the individual exposures. The data were subsequently run through the S^{4}G Pipeline 1 that mosaics them together using the Space Telescope Science Data Analysis System (STSDAS) dither package (Sheth et al. 2010; Regan et al., in preparation). Cosmic rays are eliminated in this process and the images are drizzled together to a mosaic that has 0.75 arcsec pixels (the original pixel size is about 1.2 arcsec). Sheth et al. (2010) give more details on pipeline processing. We used only the 3.6 μm mosaics to search for faint outer features. The 4.5 μm images are usually almost identical to the 3.6 μm images, but are farther from the peak of the old stellar population spectral energy distribution, and may suffer from hot dust contribution. It should be noted that the 3.6 μm band contains the 3.3 μm polycyclic aromatic hydrocarbon (PAH) emission band, while the 4.5 μm band contains a CO absorption band.

3 DETECTION AND CLASSIFICATION METHODOLOGY

We displayed each galaxy with the SAOIMAGE DS9 astronomical imaging and data visualization application (Joye & Mandel 2003), using both the histogram equalization and log scales, and in both black-and-white and rainbow colour schemes, adjusting to the extremes of contrast and sampling carefully the contrast in between the extremes. We also experimented with making unsharp-masked versions of the images, but did not use those in the final classification of the outermost features, as they did not help in the detection of the outermost features.

We can reliably classify features down to a per pixel surface brightness level of 0.03 MJy sr^{-1} (21.5 Vega mag arcsec^{-2}, 24.3 AB mag arcsec^{-2}, or about 2.5σ above the background level) based on the faintest detected structures (the polar ring candidates) and assess asymmetries in the outer isophotes at about 0.01 MJy sr^{-1} (22.7 Vega mag arcsec^{-2} or 25.5 AB mag arcsec^{-2}) level at 3.6 μm.

The first author of this paper looked at every galaxy, and five of the coauthors of this paper looked at a few dozen to hundreds of separate galaxies each, so that each galaxy was checked by at least two persons. The detected features were iterated upon until all the classifiers that looked at any given feature agreed. Immediate agreement was found for more than two-third of the features. The whole team of authors of this paper discussed the detected features, and a consensus was formed on the discovered features reported in this paper.

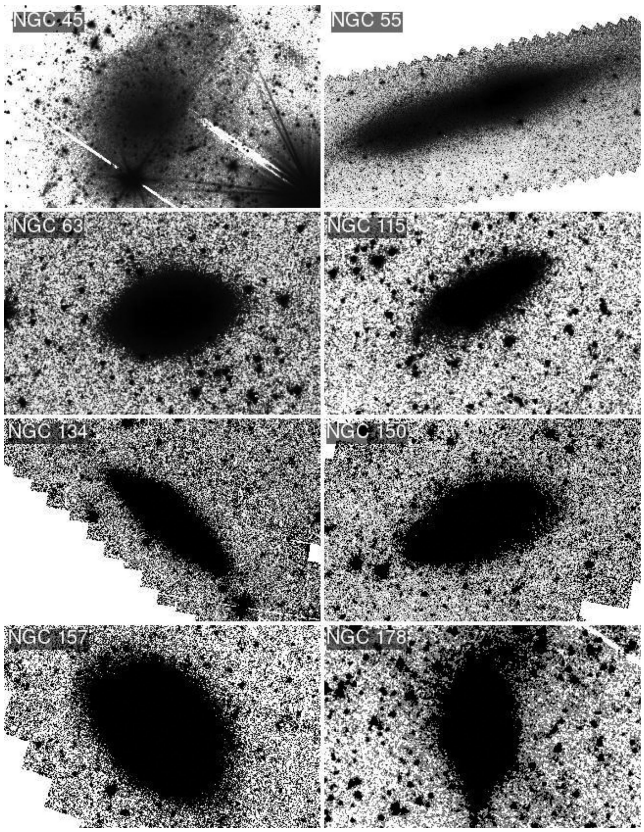

Figure 1. Images of asymmetric outer discs in the S^{4}G sample. Images of all detected asymmetric outer discs are available in the online version of the journal.

We searched for eight kinds of features (in no case was the same feature classified as belonging to two or more different classes listed below, and every feature was classified as belonging uniquely to one of the following classes).

(i) Asymmetries of the *outer* isophotes. If the outermost visible isophotes were not elliptical, we called the galaxy 'asymmetric'. Irregular outer isophotes were not a sufficient reason to classify a galaxy asymmetric if the overall outer isophote appearance was elliptical. We did not have any cases of symmetric boxy isophotes that we would call an asymmetry by our rule. However, if the nucleus was offset or the inner parts were lopsided, but the outermost visible isophotes were smooth and elliptical, we did not call the galaxy asymmetric. Lopsidedness, based on the inner high S/N parts of a small subsample of 167 S^{4}G galaxies, is discussed in another paper (Zaritsky et al. 2013). All of the discovered outer disc asymmetries, as well as all the other features that we detected and classified, are given in Figs 1–8 and they are tabulated in Table 1 that also shows the T types and the 3.6 μm absolute AB magnitudes.

(ii) A clear extension on any 'side' of the galaxy. An 'extension' is usually a narrow feature extending clearly far out from the edge of the galaxy. In no case was the same feature called both an

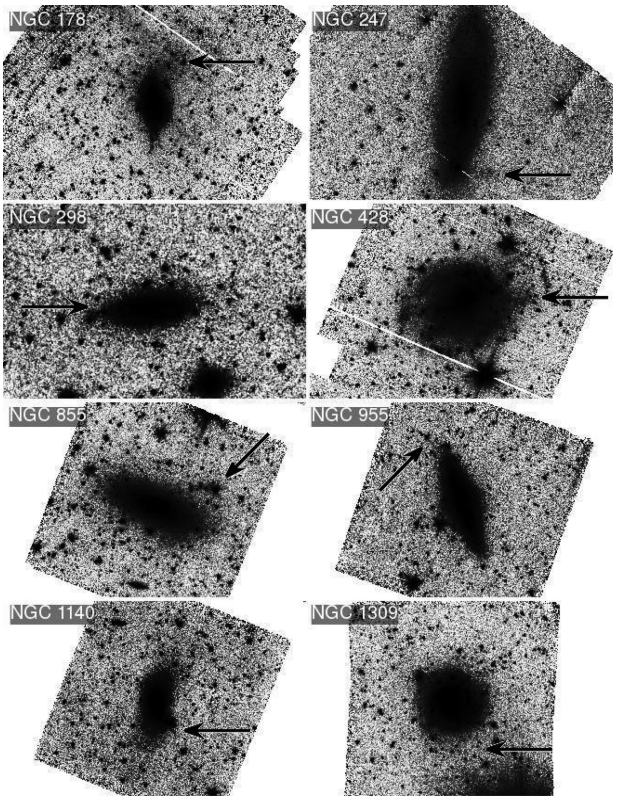

Figure 2. Images of extensions in the S^{4}G sample. Images of all detected extensions are available in the online version of the journal.

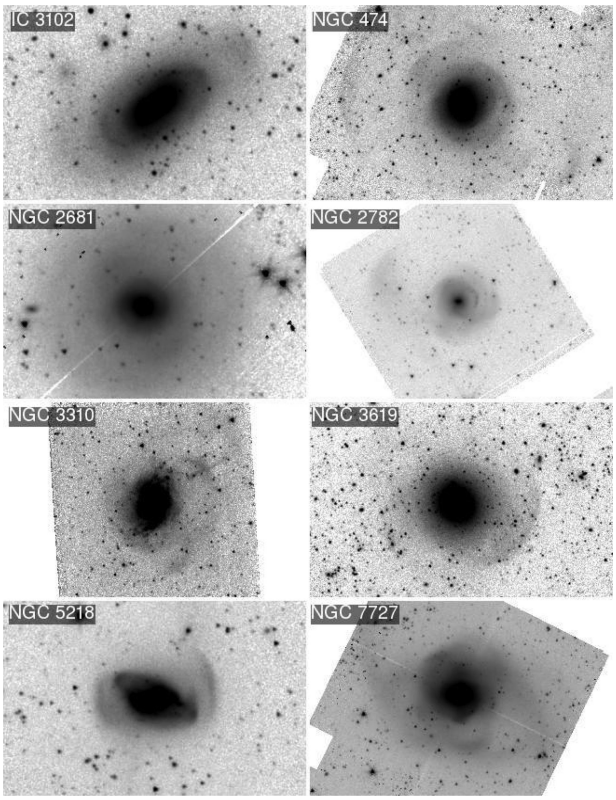

Figure 4. Images of shells in the S^{4}G sample.

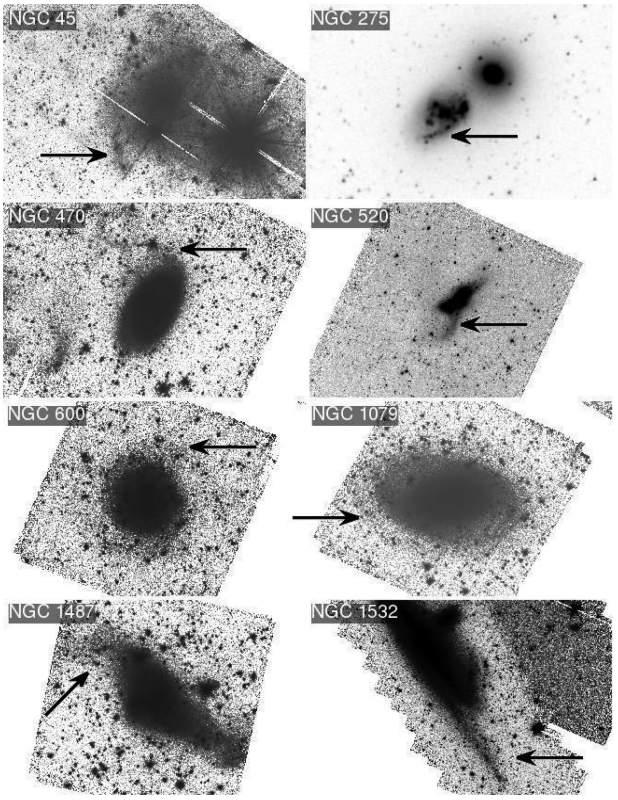

Figure 3. Images of tidal tails in the S^{4}G sample. Images of all detected tidal tails are available in the online version of the journal.

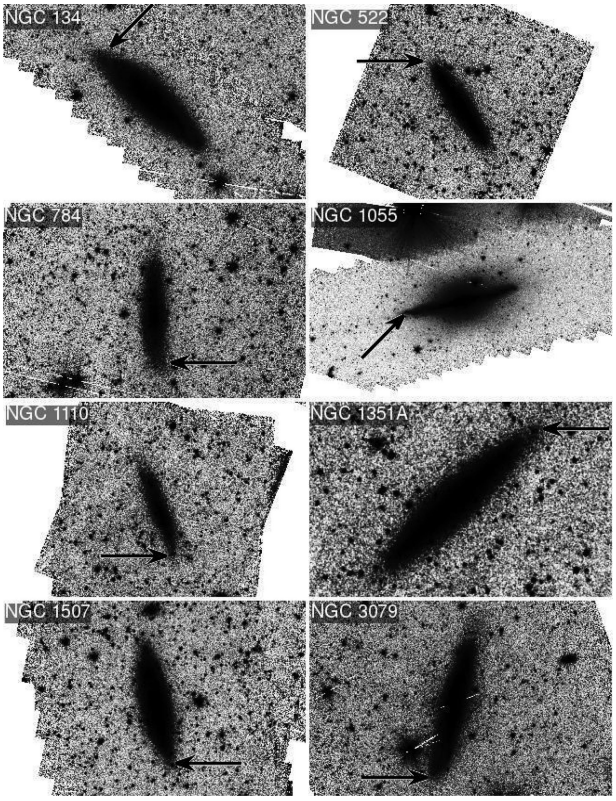

Figure 5. Images of warps in the S^{4}G sample. Images of all detected warps are available in the online version of the journal.

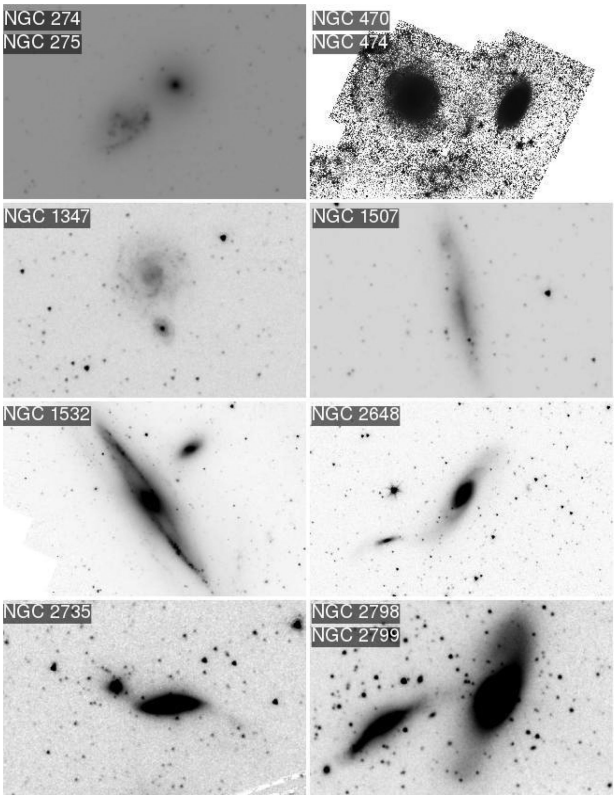

Figure 6. Images of interacting galaxies in the S^{4}G sample. Images of all detected interactions are available in the online version of the journal.

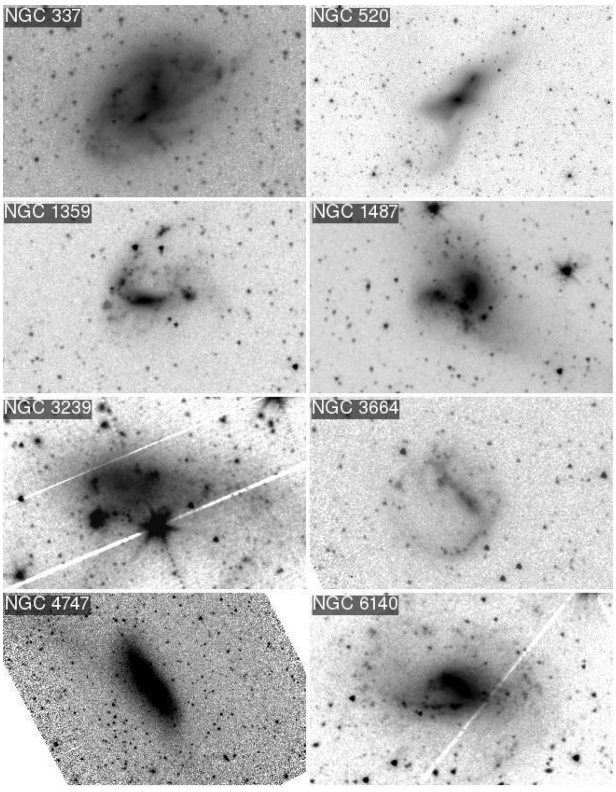

Figure 7. Images of merging galaxies in the S^{4}G sample. Images of all detected mergers are available in the online version of the journal.

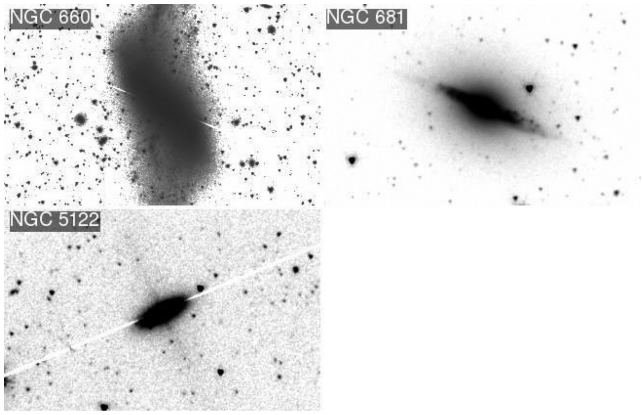

Figure 8. Images of galaxies with polar rings in the S^{4}G sample.

'asymmetry' and an 'extension'. Most extensions do not appear to be associated with spiral arms, but in a few cases spiral arms extend well outside the visible disc or main body of the galaxy, and were thus classified as 'extensions'.

(iii) Warps of the disc galaxies (for more on edge-on galaxies in the S^{4}G sample see Comerón et al. 2011, 2012). These were only looked for in galaxies that were of very high ellipticity as seen by eye. We looked for visually discernible deviations from a straight line on both sides of the centre of a galaxy and called the galaxy warped if either side (or both) showed a visually detectable curvature. We did not pay attention to the derived inclination values of the galaxies while searching for warps. Therefore, some of the elongated nearly face-on galaxies were classified as 'warped'. In Section 5 we present statistics only for truly warped galaxies (high inclination galaxies), but keep all the original warp classifications in Table 1. Warps are different from asymmetries in truly inclined galaxies, as a warped galaxy may still have a symmetric disc in its plane, but the plane itself is twisted.

(iv) Tidal tails. These are curved features outside the main bodies of the galaxies, but connecting to them in most cases. These features are usually found in galaxies that appear to be interacting or merging, but sometimes tidal-like features are seen in apparently non-interacting galaxies, and could result from past mergers. These features extend and curve around galaxies for much longer distances than extensions (usually comparable in length to half the catalogued galaxy diameter). In some cases a curvy shorter feature outside the main galaxy disc was also called a tidal tail. It is possible that some of the features classified as tidal tails are associated with outer ring features such as in NGC 1079 (Buta 1995).

(v) Shell features. Definitions of shell features are given in Athanassoula & Bosma (1985). These features exist usually around elliptical and lenticular galaxies (e.g. Malin & Carter 1980; Schweizer & Seitzer 1988). They usually have sharp, curved edges in their light distribution at their outer edge, with the concave part always pointing towards the galaxy centre. There is no reason why they should exist only around elliptical galaxies, and therefore, we searched for them in disc galaxies as well. However, there is some expectation that shells should be less likely in disc galaxies, because they arise from deeply plunging orbits that would perturb the disc. In Section 4 we discuss the differences of our detected shell features from those of Kim et al. (2012) in the S^{4}G sample.

(vi) Interacting and merging galaxies. The *revealing* and defining sign of an ongoing interaction between disc-like galaxies is a bridge or some connecting material between two galaxies. However, early-type galaxies may not have such obvious signs of interaction

Table 1. Morphological outer features of S^{4}G galaxies.

Name	T type	Abs. 3.6 μm AB mag	Classification	Name	T type	Abs. 3.6 μm AB mag	Classification
NGC 45	8	−18.90	A,TT	NGC 1325	3	−20.34	A
NGC 55	9	−999	A	NGC 1326B	10	−17.73	A
NGC 63	0	−19.53	A	NGC 1332	−3	−21.76	C
NGC 115	7	−18.68	A	NGC 1337	6	−19.25	A
NGC 134	4	−21.99	A?,W?,C	NGC 1338	6	−20.02	U
NGC 150	2	−20.70	A?	NGC 1347	8	−18.20	I
NGC 157	5	−21.38	A	NGC 1351A	5	−18.93	W
NGC 178	99	−18.13	A,E?	NGC 1357	0	−21.12	C?
NGC 216	8	−18.35	A	NGC 1359	8	−19.65	A,M?
NGC 247	8	−18.64	E,U	NGC 1367	0	−21.48	E
NGC 254	−1	−19.78	C	NGC 1385	8	−20.12	E
NGC 274	−3	−19.45	I	NGC 1406	5	−20.35	E
NGC 275	8	−19.42	TT,I	NGC 1411	−2	−20.07	C
NGC 289	2	−21.26	A,C	NGC 1414	2	−17.12	E
NGC 298	8	−18.03	E	NGC 1422	7	−18.48	E
NGC 337	6	−20.26	A,M?	NGC 1427A	10	−17.57	A
NGC 337A	9	−17.80	A	NGC 1437B	10	−17.00	C?
NGC 428	8	−19.02	E	NGC 1482	2	−20.83	E,C
NGC 470	2	−21.63	TT,I	NGC 1484	8	−17.98	E
NGC 474	0	−21.17	S,I	NGC 1487	99	−17.78	A,TT,M?
NGC 518	−1	−20.51	A	NGC 1495	8	−18.86	A
NGC 520	99	−21.45	TT,M	NGC 1507	9	−17.99	W,I,C
NGC 522	0	−21.35	W	NGC 1510	0	−16.68	C
NGC 578	6	−20.52	A	NGC 1511	5	−20.44	C
NGC 600	7	−19.19	TT	NGC 1512	1	−20.41	A,C
NGC 658	4	−20.73	A	NGC 1518	9	−18.01	A
NGC 660	2	−21.07	PR?	NGC 1532	2	−22.08	A,TT,I
NGC 672	7	−18.48	C	NGC 1546	1	−20.15	U
NGC 681	4	−21.51	PR?	NGC 1553	−1	−22.24	U
NGC 691	2	−21.44	A	NGC 1556	9	−18.03	E
NGC 772	3	−22.58	C	NGC 1559	6	−20.76	A
NGC 784	10	−16.00	A,W	NGC 1566	3	−21.12	A
NGC 855	−3	−17.52	E	NGC 1592	10	−15.77	A
NGC 864	4	−20.21	A	NGC 1596	−3	−20.22	C
NGC 865	4	−20.14	A	NGC 1602	10	−17.78	A,C
NGC 895	5	−20.67	A	NGC 1637	3	−19.59	A
NGC 908	3	−21.44	U	NGC 1679	10	−18.57	E
NGC 955	−1	−20.40	E	NGC 1688	8	−18.97	A
NGC 986	2	−20.87	A	NGC 1808	1	−21.34	A
NGC 986A	10	−16.37	A	NGC 1809	8	−18.49	A?,E,U
NGC 988	7	−19.71	U	NGC 1879	9	−18.43	A
NGC 1032	−3	−21.87	U	NGC 1892	5	−18.93	A
NGC 1047	11	−17.76	A	NGC 2101	10	−16.85	A
NGC 1055	4	−21.62	W	NGC 2460	1	−21.41	TT
NGC 1068	1	−22.70	U	NGC 2541	8	−18.26	A
NGC 1079	−1	−21.07	TT?	NGC 2543	3	−20.73	E
NGC 1084	5	−21.41	A	NGC 2552	9	−17.54	A
NGC 1087	7	−20.37	A	NGC 2608	3	−20.24	A
NGC 1090	5	−20.84	A	NGC 2633	3	−21.03	A
NGC 1097	2	−22.81	A,C	NGC 2634A	9	−18.47	C
NGC 1110	9	−17.33	W	NGC 2648	1	−21.41	A,I,C
NGC 1140	−2	−18.68	A,E	NGC 2655	0	−22.33	E
NGC 1179	6	−19.25	A	NGC 2681	0	−20.75	S?
NGC 1187	4	−20.84	C	NGC 2685	−2	−19.69	E
NGC 1222	−3	−20.35	A	NGC 2715	5	−20.52	E
NGC 1249	9	−19.01	A	NGC 2731	99	−20.25	A
NGC 1253	7	−20.17	C	NGC 2735	1	−21.00	A,TT,I,C
NGC 1255	6	−20.50	A	NGC 2748	4	−20.51	A
NGC 1258	2	−18.61	C	NGC 2750	4	−20.98	A
NGC 1300	3	−21.08	A	NGC 2764	1	−20.67	A
NGC 1309	4	−20.78	E	NGC 2770	5	−20.49	A,C
NGC 1313	7	−18.60	A,E	NGC 2776	5	−20.66	A

Table 1 – *continued*

Name	T type	Abs. 3.6 μm AB mag	Classification	Name	T type	Abs. 3.6 μm AB mag	Classification
NGC 2782	1	−20.61	E,S	NGC 3424	2	−20.91	A,C
NGC 2793	99	−18.49	A	NGC 3430	4	−20.99	A,C
NGC 2798	1	−20.68	A,I,C	NGC 3432	9	−19.03	A,C
NGC 2799	8	−18.51	A,I,C	NGC 3433	3	−20.93	TT?
NGC 2805	5	−20.44	E	NGC 3440	10	−19.11	A
NGC 2814	10	−18.65	A,C	NGC 3443	8	−17.72	E
NGC 2820	6	−20.43	C	NGC 3445	9	−18.89	C
NGC 2854	2	−20.14	A,C	NGC 3447A	9	−18.12	A,TT?,C
NGC 2894	−2	−21.35	U	NGC 3447B	10	−15.20	A,C
NGC 2964	3	−20.84	C	NGC 3448	10	−20.06	A,C
NGC 2966	1	−19.99	A,C	NGC 3455	5	−19.45	A
NGC 2968	−1	−19.78	C	NGC 3468	99	−22.72	A
NGC 2986	−5	−22.54	C	NGC 3471	0	−20.02	C
NGC 3003	7	−19.91	A,TT?	NGC 3485	4	−19.52	A
NGC 3018	8	−18.37	A,C	NGC 3488	6	−20.39	U
NGC 3020	9	−19.35	A,TT?	NGC 3495	5	−20.21	A
NGC 3023	8	−19.50	A,C	NGC 3510	7	−17.42	A,W
NGC 3024	8	−18.02	A	NGC 3513	6	−18.93	A
NGC 3026	7	−18.82	A	NGC 3521	4	−22.21	A
NGC 3027	8	−18.90	A,TT?	NGC 3526	8	−19.46	U
NGC 3034	0	−21.12	A	NGC 3547	6	−19.29	A
NGC 3044	8	−20.48	A	NGC 3583	2	−21.48	C
NGC 3049	2	−20.01	A	NGC 3589	10	−18.04	A
NGC 3057	8	−18.51	A	NGC 3596	4	−19.78	A,TT?
NGC 3061	3	−20.56	A	NGC 3600	1	−18.29	A
NGC 3065	−2	−20.96	C	NGC 3619	−5	−21.07	S
NGC 3066	2	−20.03	C	NGC 3625	7	−19.39	A
NGC 3073	−3	−18.63	C	NGC 3627	3	−21.70	A,TT
NGC 3079	3	−21.82	A,C,E,W?	NGC 3628	4	−21.73	A,W
NGC 3094	1	−21.77	A?	NGC 3631	5	−20.14	E
NGC 3104	10	−16.48	A	NGC 3633	1	−20.87	A
NGC 3118	6	−18.33	A	NGC 3642	2	−20.71	E
NGC 3153	7	−19.90	A	NGC 3652	5	−19.94	A
NGC 3162	5	−20.35	A	NGC 3664	9	−18.59	A,TT,M?
NGC 3165	9	−17.18	C	NGC 3666	4	−19.76	W?
NGC 3169	2	−21.70	A	NGC 3669	7	−20.63	A
NGC 3185	1	−20.19	A,C	NGC 3672	5	−21.49	A
NGC 3187	5	−19.53	A	NGC 3675	3	−21.84	E
NGC 3190	1	−21.80	A,C	NGC 3686	4	−20.33	A
NGC 3206	7	−18.69	A	NGC 3687	2	−19.84	C
NGC 3227	1	−21.55	A,I,C	NGC 3701	5	−20.23	A
NGC 3239	9	−17.36	A,TT,M	NGC 3705	3	−20.84	A
NGC 3245A	7	−17.75	A	NGC 3712	10	−17.00	A
NGC 3246	7	−19.37	A	NGC 3718	1	−20.88	A,TT
NGC 3264	8	−17.72	A	NGC 3726	4	−20.87	A
NGC 3294	4	−21.54	A	NGC 3729	0	−20.41	A
NGC 3306	3	−20.75	TT	NGC 3733	5	−19.27	TT,U
NGC 3310	4	−20.59	A,E,S	NGC 3735	5	−22.04	A
NGC 3320	5	−20.31	U	NGC 3755	5	−19.74	A
NGC 3321	6	−20.23	A	NGC 3769	6	−19.38	C
NGC 3338	4	−21.10	A	NGC 3779	9	−17.18	A
NGC 3359	7	−20.41	A	NGC 3780	5	−21.77	A
NGC 3364	4	−20.40	A	NGC 3782	9	−17.68	U
NGC 3365	7	−18.65	A	NGC 3786	0	−21.50	I,C
NGC 3368	−1	−21.35	TT,U	NGC 3788	1	−21.67	A,I,C
NGC 3377A	10	−15.30	C	NGC 3846A	9	−18.43	A,TT
NGC 3381	8	−19.45	A	NGC 3850	9	−17.61	A
NGC 3384	−3	−20.74	TT,C	NGC 3876	8	−19.68	C
NGC 3389	5	−19.77	A	NGC 3877	4	−20.72	A
NGC 3395	5	−19.90	A,TT?,I,C	NGC 3885	−1	−21.29	U
NGC 3396	10	−19.61	A,I,C	NGC 3887	4	−20.87	A
NGC 3414	−3	−21.75	C	NGC 3888	3	−21.27	A

Table 1 – *continued*

Name	T type	Abs. 3.6 μm AB mag	Classification	Name	T type	Abs. 3.6 μm AB mag	Classification
NGC 3896	9	−17.44	C,U	NGC 4283	−5	−19.30	C
NGC 3912	9	−19.71	A	NGC 4288	9	−17.75	A
NGC 3917	5	−19.62	C	NGC 4293	0	−20.72	A
NGC 3930	7	−18.64	E	NGC 4294	7	−19.19	C
NGC 3938	5	−20.98	A	NGC 4298	4	−20.17	I?,C
NGC 3949	6	−20.36	A?	NGC 4299	9	−18.36	C
NGC 3952	10	−18.49	A	NGC 4302	4	−21.41	I?,E,C,W?
NGC 3956	6	−19.85	A,C	NGC 4303A	8	−17.68	E
NGC 3962	−4	−22.35	U	NGC 4309	−1	−18.46	C
NGC 3972	5	−19.39	E	NGC 4313	1	−19.94	C
NGC 3976	4	−21.58	A	NGC 4319	1	−20.83	TT,C
NGC 3981	4	−20.97	A	NGC 4321	4	−21.99	C
NGC 3982	3	−20.40	A	NGC 4343	1	−20.65	C
NGC 3992	2	−22.39	C	NGC 4355	0	−19.31	C
NGC 3998	−2	−21.70	C	NGC 4388	2	−21.26	C
NGC 4010	8	−19.54	A	NGC 4393	9	−16.99	U
NGC 4020	8	−16.73	A	NGC 4394	0	−20.53	TT,C
NGC 4027	8	−21.25	A,C	NGC 4395	8	−17.04	A
NGC 4038	99	−21.97	TT,I,C	NGC 4402	5	−20.28	C
NGC 4039	99	−20.79	TT,I,C	NGC 4406	−4	−999	U
NGC 4049	9	−16.78	A	NGC 4411A	7	−17.75	TT,C
NGC 4051	3	−20.84	A	NGC 4423	9	−18.03	W
NGC 4088	5	−21.22	A	NGC 4438	0	−21.22	A,C
NGC 4094	6	−19.87	U	NGC 4472	−5	−23.12	C
NGC 4096	7	−20.24	A	NGC 4485	10	−17.47	A,I,C
NGC 4105	−5	−999	I,U,C	NGC 4488	1	−18.92	A,TT?
NGC 4106	1	−22.40	A,I,C	NGC 4490	9	−19.73	A,I,C
NGC 4108	5	−20.67	C,U	NGC 4496A	7	−19.19	U
NGC 4111	−3	−20.70	E	NGC 4503	10	−20.54	C
NGC 4117	−3	−18.81	C	NGC 4517A	8	−18.71	A
NGC 4123	3	−20.41	A	NGC 4519	7	−20.21	A
NGC 4141	8	−17.92	TT	NGC 4523	9	−17.39	U
NGC 4144	9	−17.25	W	NGC 4532	10	−19.06	A
NGC 4151	0	−19.87	E?	NGC 4533	7	−18.38	C
NGC 4157	5	−21.60	A?,E	NGC 4534	9	−17.71	A
NGC 4163	11	−13.83	E?	NGC 4535	5	−21.44	A
NGC 4165	3	−19.82	C?	NGC 4536	4	−21.02	A
NGC 4173	9	−15.64	A	NGC 4559	6	−19.69	A
NGC 4183	6	−18.86	E,W	NGC 4561	7	−17.36	A
NGC 4190	10	−14.09	E?	NGC 4562	8	−16.82	A?
NGC 4192	2	−21.54	A	NGC 4567	4	−21.05	I?,C
NGC 4193	2	−20.89	A?	NGC 4568	5	−21.57	I?,C
NGC 4194	1	−21.45	E	NGC 4571	5	−20.29	C,U
NGC 4197	8	−19.79	E	NGC 4572	6	−19.16	A
NGC 4204	8	−16.67	A	NGC 4594	−1	−22.64	U
NGC 4212	3	−20.63	A	NGC 4597	8	−18.65	A,C
NGC 4216	2	−22.03	C	NGC 4605	10	−18.27	A,U
NGC 4217	5	−21.45	U	NGC 4625	9	−17.28	A
NGC 4222	7	−19.43	C	NGC 4631	7	−20.20	A,E?,C
NGC 4224	−1	−21.85	C	NGC 4633	6	−18.46	C
NGC 4234	9	−19.87	A	NGC 4634	7	−16.42	A,C
NGC 4235	−1	−20.98	A	NGC 4636	−4	−999	U
NGC 4236	9	−999	A,E	NGC 4639	2	−20.42	C
NGC 4237	3	−20.54	E	NGC 4647	6	−999	A,C,U
NGC 4238	5	−19.34	C	NGC 4651	3	−21.73	TT
NGC 4244	7	−17.85	U	NGC 4653	5	−20.58	A?,C
NGC 4252	7	−16.14	A	NGC 4654	6	−20.91	A
NGC 4254	5	−21.61	A	NGC 4656	8	−17.16	A
NGC 4256	0	−22.05	C	NGC 4659	−2	−17.47	U
NGC 4258	2	−21.33	U	NGC 4666	5	−21.90	C
NGC 4268	−1	−20.13	C	NGC 4688	8	−18.37	A,E?
NGC 4273	5	−21.41	A,C	NGC 4698	0	−21.69	E?

Table 1 – *continued*

Name	T type	Abs. 3.6 μm AB mag	Classification	Name	T type	Abs. 3.6 μm AB mag	Classification
NGC 4700	9	−18.69	A	NGC 5477	10	−14.64	U
NGC 4707	10	−14.78	U	NGC 5480	7	−20.46	A,C
NGC 4723	10	−16.30	U	NGC 5481	−4	−20.50	C
NGC 4725	1	−21.76	A	NGC 5506	0	−21.18	C,U
NGC 4731	7	−19.85	A	NGC 5529	2	−22.20	W
NGC 4747	9	−18.36	A,M	NGC 5534	1	−20.37	C
NGC 4762	−2	−21.64	U	NGC 5560	7	−19.65	A,C
NGC 4775	6	−20.29	U	NGC 5566	1	−21.79	A,C
NGC 4789A	10	−12.69	A	NGC 5569	9	−17.45	E,C
NGC 4793	5	−21.41	A,C	NGC 5574	0	−19.86	I,C
NGC 4795	1	−21.40	A,TT?,I?,C	NGC 5576	−5	−21.49	I,C
NGC 4802	−2	−18.86	U	NGC 5584	7	−20.31	A
NGC 4809	10	−17.26	A	NGC 5597	7	−21.23	A
NGC 4814	4	−21.49	TT?	NGC 5600	8	−22.92	A?
NGC 4899	5	−20.72	A	NGC 5608	10	−17.27	A?
NGC 4902	3	−22.21	A	NGC 5636	0	−18.87	C
NGC 4904	6	−19.91	A	NGC 5645	8	−19.43	A
NGC 4948A	9	−18.30	E?	NGC 5660	5	−21.07	E
NGC 4951	3	−19.62	U	NGC 5661	6	−19.93	A,C
NGC 4958	−1	−21.13	A	NGC 5665	7	−20.41	A?
NGC 4961	5	−20.04	C	NGC 5669	7	−20.01	A
NGC 4981	4	−20.82	TT	NGC 5678	3	−21.61	E,C
NGC 4995	2	−21.50	U	NGC 5708	5	−20.05	A
NGC 5018	−4	−22.62	E,C	NGC 5719	0	−21.35	A
NGC 5022	3	−21.10	A,C	NGC 5730	7	−19.64	W?
NGC 5033	6	−22.04	A?	NGC 5731	9	−18.94	A
NGC 5042	6	−19.52	U	NGC 5740	2	−20.81	TT
NGC 5054	4	−21.38	C	NGC 5746	0	−22.81	U
NGC 5055	4	−21.59	E,U	NGC 5750	0	−21.44	A
NGC 5078	3	−22.71	C	NGC 5757	2	−21.59	C
NGC 5079	4	−20.05	C	NGC 5768	5	−19.99	A
NGC 5084	0	−21.94	A	NGC 5775	5	−21.60	C
NGC 5085	4	−21.73	A	NGC 5777	0	−21.75	C
NGC 5103	−3	−19.51	U	NGC 5792	2	−21.60	U
NGC 5107	10	−17.72	A	NGC 5809	1	−20.23	A
NGC 5112	7	−20.08	A	NGC 5846	−4	−22.69	C,U
NGC 5122	−3	−20.28	PR?	NGC 5850	2	−21.32	C
NGC 5145	−1	−21.26	U	NGC 5892	6	−20.48	A?
NGC 5169	5	−19.40	C	NGC 5900	3	−21.95	TT
NGC 5194	4	−21.93	I,C	NGC 5915	8	−20.36	C
NGC 5195	0	−20.57	A,E,I,C	NGC 5916	1	−20.53	A
NGC 5205	2	−19.75	E?	NGC 5916A	10	−18.60	A
NGC 5216	−5	−21.25	E?,I,C	NGC 5921	3	−20.72	A?,U
NGC 5218	1	−21.86	S,I,C	NGC 5930	0	−20.96	C,I
NGC 5240	3	−20.69	U	NGC 5953	−1	−20.62	I,C
NGC 5247	5	−21.81	E	NGC 5954	3	−20.19	I,C
NGC 5248	4	−21.43	U	NGC 5963	5	−19.89	A?,U
NGC 5297	4	−21.18	C	NGC 5981	−1	−20.48	C?
NGC 5320	5	−20.51	A	NGC 5985	3	−22.36	TT?
NGC 5334	6	−20.68	TT?	NGC 6012	2	−19.83	U
NGC 5348	7	−18.36	W?	NGC 6070	5	−21.55	A
NGC 5350	3	−21.16	C,U	NGC 6140	7	−19.32	E,M?
NGC 5353	−1	−22.35	I,C	NGC 6168	8	−19.98	A
NGC 5354	−4	−22.16	I,C	NGC 6237	9	−17.58	E
NGC 5355	−3	−19.90	C	NGC 6239	9	−19.32	A
NGC 5383	2	−21.71	A,E,C	NGC 6278	−2	−21.21	C
NGC 5403	2	−21.63	W,C	NGC 6340	0	−20.92	C,U
NGC 5426	5	−21.28	I,C	NGC 6861E	8	−18.59	A
NGC 5427	4	−21.60	I,C	NGC 6925	3	−21.82	E?
NGC 5448	1	−21.50	A	NGC 7059	7	−20.61	A
NGC 5457	5	−21.38	TT	NGC 7064	8	−17.10	A
NGC 5468	6	−21.29	E	NGC 7090	8	−18.93	U

Table 1 – *continued*

Name	T type	Abs. 3.6 μm AB mag	Classification	Name	T type	Abs. 3.6 μm AB mag	Classification
NGC 7140	3	−21.40	E	UGC 4169	6	−19.08	E
NGC 7162A	8	−19.11	U	UGC 4238	8	−18.38	U
NGC 7167	6	−19.78	U	UGC 4305	10	−15.58	A
NGC 7183	0	−21.79	A	UGC 4393	10	−18.04	A
NGC 7188	3	−18.59	A	UGC 4426	10	−14.07	A
NGC 7213	−2	−22.25	C	UGC 4483	10	−12.05	A
NGC 7307	7	−19.62	A	UGC 4499	9	−16.62	E
NGC 7347	6	−19.96	W?	UGC 4543	9	−17.91	A
NGC 7361	8	−18.69	A	UGC 4551	−1	−20.14	A
NGC 7412	4	−19.24	A	UGC 4704	8	−15.38	W
NGC 7418A	3	−17.82	E	UGC 4722	9	−16.60	A,TT
NGC 7424	6	−19.60	A?,U	UGC 4797	10	−17.19	U
NGC 7456	6	−19.12	A	UGC 4834	10	−16.74	A
NGC 7462	9	−18.42	U	UGC 4837	10	−17.26	U
NGC 7463	6	−20.13	E,C	UGC 4841	6	−19.05	U
NGC 7465	−2	−20.17	A,C	UGC 4867	7	−18.36	U
NGC 7479	3	−22.31	E	UGC 4871	9	−17.27	U
NGC 7496	3	−19.73	A?,U	UGC 4970	7	−19.22	W
NGC 7531	1	−20.73	TT	UGC 5050	8	−18.71	TT
NGC 7537	5	−20.33	C	UGC 5139	10	−999	U
NGC 7541	5	−21.96	C	UGC 5179	−2	−17.14	C
NGC 7552	1	−21.33	A	UGC 5336	10	−12.66	U
NGC 7590	4	−21.13	E	UGC 5340	10	−13.29	A
NGC 7599	6	−20.61	A,C	UGC 5364	10	−999	U
NGC 7625	1	−20.44	A	UGC 5391	8	−17.19	A,U
NGC 7694	10	−19.19	C	UGC 5421	10	−14.71	U
NGC 7714	1	−20.62	TT,C	UGC 5459	8	−19.49	E
NGC 7715	99	−18.34	E,C	UGC 5464	10	−15.35	U
NGC 7727	1	−21.66	TT?,S?,M?,U	UGC 5478	9	−17.31	U
NGC 7731	2	−19.56	C	UGC 5522	5	−18.78	A
NGC 7732	8	−19.37	A,C	UGC 5571	10	−13.84	U
NGC 7741	6	−19.28	U	UGC 5633	7	−17.73	U
NGC 7755	4	−21.17	A	UGC 5677	10	−15.85	E?
NGC 7757	6	−20.34	E	UGC 5688	10	−18.53	A,E?
NGC 7800	10	−18.79	A	UGC 5689	7	−20.01	W?
UGC 17	10	−15.69	U	UGC 5707	7	−18.19	A
UGC 99	9	−17.33	U	UGC 5708	8	−17.21	E
UGC 156	10	−16.83	A	UGC 5764	10	−13.00	E
UGC 191	8	−16.81	A?	UGC 5791	9	−15.67	E
UGC 260	6	−19.78	A,C	UGC 5829	10	−15.64	E
UGC 634	10	−17.28	U	UGC 5832	9	−17.62	A
UGC 711	9	−17.63	U	UGC 5844	9	−16.07	A
UGC 882	10	−17.40	A,U	UGC 5918	10	−13.55	U
UGC 891	9	−14.94	A	UGC 5947	10	−16.65	A
UGC 903	2	−21.33	A	UGC 5958	7	−18.20	C
UGC 941	10	−17.47	A?,U	UGC 5979	10	−16.54	E
UGC 958	8	−17.15	W	UGC 5989	8	−17.08	A
UGC 1014	10	−17.53	I	UGC 6104	6	−18.97	TT?
UGC 1133	10	−16.14	U	UGC 6145	10	−13.73	U
UGC 1176	10	−15.39	A	UGC 6151	10	−16.86	U
UGC 1195	9	−16.53	A	UGC 6157	8	−18.72	A
UGC 1197	9	−17.80	A	UGC 6171	9	−16.87	U
UGC 1547	9	−18.30	E?,C,U	UGC 6181	10	−15.94	U
UGC 1670	9	−16.40	U	UGC 6307	9	−18.26	I?
UGC 1839	9	−16.61	A?	UGC 6309	5	−20.70	A
UGC 1862	5	−18.21	U	UGC 6341	10	−15.97	C
UGC 1981	10	−16.21	U	UGC 6345	10	−17.78	A,E?
UGC 2275	10	−15.95	U	UGC 6355	8	−17.92	C
UGC 2302	9	−16.44	U	UGC 6378	8	−17.17	E?
UGC 2345	9	−16.53	A	UGC 6433	10	−17.90	A?
UGC 3070	9	−18.17	U	UGC 6446	7	−16.97	U
UGC 4121	9	−16.18	U	UGC 6534	9	−17.95	A

Table 1 – *continued*

Name	T type	Abs. 3.6 μm AB mag	Classification	Name	T type	Abs. 3.6 μm AB mag	Classification
UGC 6628	9	−17.85	U	UGC 8246	8	−16.98	A,E
UGC 6670	8	−17.63	E	UGC 8303	10	−17.44	A
UGC 6682	9	−17.25	U	UGC 8320	10	−14.60	U
UGC 6747	10	−15.39	W	UGC 8365	10	−17.18	E
UGC 6780	6	−18.64	E	UGC 8441	10	−17.47	U
UGC 6782	10	−14.64	U	UGC 8449	8	−16.28	A
UGC 6816	9	−17.15	A	UGC 8489	9	−17.00	TT?
UGC 6817	10	−12.81	U	UGC 8508	10	−12.50	E?
UGC 6849	8	−16.54	A	UGC 8597	8	−18.60	TT?
UGC 6903	6	−19.46	U	UGC 8614	10	−18.77	U
UGC 6912	10	−17.25	U	UGC 8630	9	−19.16	A
UGC 6955	10	−17.45	U	UGC 8639	10	−17.48	A
UGC 6956	9	−16.38	E	UGC 8642	9	−16.68	A
UGC 6969	10	−16.82	A,C	UGC 8688	10	−17.23	U
UGC 6983	7	−18.31	A?	UGC 8726	8	−17.49	E
UGC 7019	10	−16.96	C,U	UGC 8733	8	−18.73	C
UGC 7053	10	−16.26	U	UGC 8877	8	−17.58	C,U
UGC 7089	9	−17.21	A	UGC 8892	8	−17.58	U
UGC 7094	10	−15.77	E	UGC 8995	6	−17.73	TT?
UGC 7125	10	−16.82	E	UGC 9057	7	−18.33	A,TT
UGC 7170	7	−18.02	W?	UGC 9126	10	−17.51	U
UGC 7175	10	−16.56	A	UGC 9128	10	−12.57	U
UGC 7189	7	−18.52	U	UGC 9169	9	−16.76	A,TT?
UGC 7218	10	−16.22	U	UGC 9206	10	−18.59	U
UGC 7242	99	−999	U	UGC 9242	6	−17.11	E
UGC 7257	10	−16.67	A,C	UGC 9245	8	−16.68	A
UGC 7271	8	−14.73	A	UGC 9249	8	−16.52	A
UGC 7300	10	−14.43	U	UGC 9310	8	−17.94	A
UGC 7321	7	−17.68	A	UGC 9469	9	−17.05	U
UGC 7332	10	−16.05	U	UGC 9760	8	−16.38	E,W?
UGC 7396	8	−17.68	A?	UGC 9815	8	−17.70	W
UGC 7408	10	−15.01	U	UGC 9837	6	−19.40	A?,U
UGC 7534	10	−16.45	U	UGC 9845	7	−17.23	U
UGC 7557	8	−16.97	U	UGC 9856	7	−17.84	W
UGC 7559	10	−13.68	U	UGC 9858	3	−20.58	E,C
UGC 7590	9	−18.25	U	UGC 9875	9	−17.72	U
UGC 7599	10	−13.01	U	UGC 9936	9	−18.05	A
UGC 7605	10	−13.03	U	UGC 10014	10	−17.06	U
UGC 7608	10	−14.42	U	UGC 10041	8	−19.04	E
UGC 7639	11	−15.06	A	UGC 10043	1	−20.75	W,C
UGC 7673	10	−14.77	U	UGC 10054	7	−18.13	A
UGC 7698	10	−14.97	U	UGC 10061	10	−17.17	A
UGC 7699	7	−17.62	A	UGC 10194	8	−16.09	A,E
UGC 7700	9	−18.82	C,U	UGC 10288	5	−20.51	E?
UGC 7719	10	−14.79	A	UGC 10310	10	−16.72	A,C
UGC 7730	7	−17.51	A	UGC 10437	9	−18.33	E
UGC 7795	10	−10.74	U	UGC 10445	8	−18.74	A
UGC 7802	7	−17.59	W?	UGC 10477	8	−15.54	A,W?
UGC 7906	10	−14.86	U	UGC 10608	10	−15.57	A
UGC 7911	8	−18.45	U	UGC 10650	10	−18.33	A,U
UGC 7949	10	−999	U	UGC 10736	8	−15.59	U
UGC 8040	3	−19.72	A,C	UGC 10806	8	−17.59	A
UGC 8052	5	−18.54	A?	UGC 10854	9	−17.71	A
UGC 8053	9	−16.72	U	UGC 11782	10	−16.92	A
UGC 8056	7	−17.87	U	UGC 12178	8	−19.34	E
UGC 8084	9	−18.64	U	UGC 12313	9	−16.93	A?,C
UGC 8127	9	−16.10	A,C	UGC 12350	8	−17.98	U
UGC 8146	8	−16.94	A	UGC 12578	10	−17.87	A,E
UGC 8153	7	−18.54	U	UGC 12613	10	−13.38	U
UGC 8155	1	−19.95	E	UGC 12681	9	−17.53	A
UGC 8166	8	−17.21	E	UGC 12682	10	−17.32	A
UGC 8201	10	−14.41	U	UGC 12709	9	−18.41	U

Table 1 – *continued*

Name	T type	Abs. 3.6 μm AB mag	Classification	Name	T type	Abs. 3.6 μm AB mag	Classification
UGC 12732	8	−16.61	U	IC 4901	5	−20.40	A
UGC 12843	7	−18.03	U	IC 4986	8	−18.17	U
UGC 12856	9	−17.55	A	IC 5007	8	−20.22	A
UGC 12857	3	−19.74	W	IC 5152	11	−15.31	U
IC 167	6	−18.66	TT,C	IC 5176	4	−20.90	E
IC 223	10	−16.92	A	IC 5201	7	−19.06	A
IC 600	9	−17.89	E	IC 5249	7	−18.31	A,W
IC 718	9	−18.17	A	IC 5269A	9	−18.28	A
IC 749	6	−20.51	A,C	IC 5269C	8	−17.82	A
IC 750	1	−21.35	C	IC 5273	6	−19.77	A
IC 755	9	−18.38	A	IC 5332	6	−18.93	U
IC 764	5	−20.04	A	ESO 011−005	8	−18.98	E
IC 1024	9	−19.15	A	ESO 012−010	7	−18.70	A
IC 1029	1	−21.79	C	ESO 012−014	10	−16.89	A
IC 1066	4	−19.52	C	ESO 015−001	10	−16.74	A
IC 1067	3	−19.38	E,C	ESO 027−001	4	−19.80	E
IC 1125	8	−19.55	A	ESO 027−008	4	−20.77	A
IC 1151	7	−20.02	A	ESO 048−017	9	−17.63	A
IC 1210	1	−20.29	A	ESO 054−021	8	−18.64	E
IC 1251	10	−17.30	A	ESO 079−003	1	−21.35	A,W?,U
IC 1553	6	−19.65	A	ESO 085−047	9	−16.00	U
IC 1555	8	−17.38	A	ESO 107−016	8	−16.95	A
IC 1558	8	−17.34	A	ESO 114−007	10	−17.41	A
IC 1596	4	−19.06	A	ESO 115−021	9	−15.25	A
IC 1613	10	−999	U	ESO 116−012	9	−999	U
IC 1727	9	−16.87	A,C	ESO 119−016	8	−17.46	I?
IC 1826	10	−20.17	U	ESO 120−012	10	−16.72	A
IC 1870	9	−18.27	A,U	ESO 120−021	10	−15.16	A
IC 1892	8	−18.82	A?,U	ESO 145−025	9	−17.05	A
IC 1952	6	−19.37	U	ESO 146−014	8	−16.44	A
IC 1962	9	−16.65	TT	ESO 149−001	7	−18.27	A
IC 1993	2	−18.79	U	ESO 149−003	10	−13.27	A
IC 2032	10	−15.50	A	ESO 150−005	7	−16.82	U
IC 2389	9	−18.82	A?	ESO 154−023	8	−16.17	A
IC 2461	−2	−21.21	E	ESO 159−025	10	−15.17	A
IC 2574	10	−16.99	A?,E?	ESO 187−035	9	−16.67	A
IC 2627	4	−19.81	A,E	ESO 187−051	9	−16.10	A
IC 2763	8	−17.01	C	ESO 202−035	5	−19.28	A
IC 2963	8	−18.19	A	ESO 202−041	9	−15.49	A
IC 2996	6	−18.87	U	ESO 234−043	8	−17.66	A
IC 3102	0	−20.57	A,S	ESO 236−039	10	−15.84	A
IC 3105	10	−15.49	A	ESO 240−004	9	−15.86	A
IC 3155	−2	−19.14	C	ESO 245−005	10	−14.38	U
IC 3258	10	−16.99	U	ESO 249−035	9	−14.79	C
IC 3268	10	−18.14	U	ESO 249−036	10	−14.62	U
IC 3322A	7	−20.00	W?	ESO 285−048	7	−19.33	A
IC 3355	10	−9.68	A	ESO 287−037	8	−19.07	A
IC 3356	10	−15.55	U	ESO 289−026	7	−17.70	A
IC 3371	8	−17.23	E?	ESO 289−048	7	−18.12	E
IC 3475	11	−19.18	U	ESO 292−014	7	−19.28	W?
IC 3522	10	−15.46	A?	ESO 293−034	99	−19.70	A,W?,C
IC 3576	9	−16.89	U	ESO 302−014	8	−13.90	U
IC 3583	10	−17.22	A,E?	ESO 302−021	9	−13.28	TT?
IC 3611	9	−19.02	A	ESO 305−009	8	−16.79	U
IC 3687	10	−13.75	A	ESO 305−017	10	−15.66	TT?
IC 3742	8	−17.85	A	ESO 340−017	7	−19.10	A
IC 3881	8	−17.10	E	ESO 340−042	8	−18.37	A?,U
IC 4351	3	−21.87	W	ESO 341−032	9	−19.14	A
IC 4214	0	−21.44	E	ESO 342−050	4	−20.42	A
IC 4407	9	−18.29	A	ESO 345−046	7	−18.66	E?,C
IC 4468	4	−20.25	A	ESO 346−014	7	−18.36	U
IC 4582	4	−20.33	A	ESO 347−008	9	−9.69	U

Table 1 – *continued*

Name	T type	Abs. 3.6 μm AB mag	Classification	Name	T type	Abs. 3.6 μm AB mag	Classification
ESO 347−029	5	−18.01	U	ESO 505−003	9	−18.55	W
ESO 357−007	9	−15.98	A	ESO 505−008	7	−17.65	E?
ESO 357−012	8	−17.89	A?,U	ESO 505−009	6	−16.90	U
ESO 358−015	9	−15.88	A?	ESO 505−013	7	−18.76	A
ESO 358−020	10	−17.39	E?	ESO 505−023	9	−16.06	A
ESO 358−054	9	−16.83	A	ESO 506−029	8	−18.69	A
ESO 358−060	10	−12.99	U	ESO 508−007	8	−17.42	U
ESO 358−063	5	−20.16	A	ESO 508−015	10	−18.19	A
ESO 359−003	9	−16.58	U	ESO 508−019	9	−19.04	A,TT?
ESO 359−031	10	−16.45	A	ESO 508−024	5	−20.19	A
ESO 361−009	10	−15.08	U	ESO 508−030	10	−16.09	A,C?
ESO 361−019	10	−18.16	A	ESO 510−026	10	−17.85	U
ESO 362−011	4	−19.86	A	ESO 510−058	9	−19.60	C
ESO 362−019	8	−16.44	E	ESO 510−059	5	−19.24	A,C
ESO 399−025	−5	−20.19	U	ESO 532−014	7	−16.13	A,TT
ESO 402−025	9	−17.50	C	ESO 532−022	7	−17.93	A,TT
ESO 402−026	2	−21.76	C	ESO 539−007	9	−16.79	U
ESO 404−003	6	−19.09	A	ESO 540−031	10	−11.50	A
ESO 404−017	9	−17.99	A	ESO 541−005	9	−16.58	A
ESO 404−027	2	−20.00	A	ESO 545−005	3	−19.52	A,E
ESO 406−042	10	−16.72	A	ESO 545−016	8	−16.69	A
ESO 407−007	0	−20.26	U	ESO 547−012	9	−15.99	E?
ESO 407−018	10	−11.96	U	ESO 547−020	10	−16.77	A
ESO 408−012	9	−18.68	U	ESO 548−005	9	−17.57	U
ESO 409−015	10	−13.69	A	ESO 548−009	8	−17.71	U
ESO 410−012	9	−14.72	A	ESO 548−016	1	−17.35	TT,C
ESO 411−013	9	−15.70	U	ESO 548−032	8	−17.46	A
ESO 420−006	10	−15.21	U	ESO 548−082	10	−16.17	U
ESO 422−033	10	−16.31	U	ESO 549−002	10	−15.82	U
ESO 438−017	7	−17.24	U	ESO 549−018	3	−19.87	A
ESO 440−004	8	−19.09	A,TT	ESO 549−035	9	−16.31	A
ESO 440−044	10	−16.37	E	ESO 550−005	7	−16.81	W?
ESO 440−046	8	−17.42	E	ESO 551−016	8	−16.56	U
ESO 440−049	5	−18.16	A	ESO 553−017	8	−16.98	U
ESO 441−014	9	−17.81	C	ESO 567−048	9	−14.13	U
ESO 443−069	8	−20.01	A	ESO 569−014	7	−19.13	E
ESO 443−079	9	−16.58	A,E?	ESO 572−030	9	−17.56	A
ESO 443−080	9	−18.31	A	ESO 573−003	10	−999	U
ESO 443−085	7	−17.61	E?	ESO 576−001	1	−21.26	C
ESO 444−033	9	−17.75	E	ESO 576−005	7	−18.47	U
ESO 444−037	10	−17.56	A	ESO 576−008	1	−19.25	U
ESO 444−078	10	−999	A,U	ESO 576−040	8	−17.90	E
ESO 445−089	7	−19.96	A	ESO 576−050	7	−19.22	E
ESO 462−031	−1	−19.18	C	ESO 576−059	9	−17.00	U
ESO 466−036	−5	−20.03	A?	ESO 577−038	9	−15.96	E
ESO 467−051	9	−16.57	C	ESO 580−034	7	−17.59	A,C
ESO 469−008	9	−16.12	A	ESO 582−004	2	−18.07	U
ESO 476−010	10	−16.23	A	ESO 601−025	9	−17.58	A
ESO 479−025	9	−17.83	I	ESO 601−031	9	−17.20	A?,U
ESO 480−020	5	−16.05	C,U	ESO 602−003	10	−17.67	A
ESO 481−014	8	−17.29	TT?	PGC 143	10	−999	U
ESO 482−005	7	−17.18	E	PGC 2689	10	−16.83	U
ESO 485−021	6	−17.43	TT	PGC 2805	9	−16.45	A,E?
ESO 486−003	10	−16.18	A?	PGC 3855	9	−17.16	U
ESO 486−021	10	−15.22	TT	PGC 4143	11	−16.99	U
ESO 501−079	10	−999	U	PGC 6244	9	−16.48	A
ESO 501−080	9	−16.95	A	PGC 6626	6	−17.66	U
ESO 502−016	9	−16.91	A	PGC 7900	8	−17.64	A,U
ESO 502−020	7	−17.36	A	PGC 8295	8	−17.47	E
ESO 502−023	10	−15.32	U	PGC 8962	10	−16.66	W?
ESO 504−028	6	−18.48	A	PGC 12068	9	−17.92	A
ESO 505−002	10	−17.44	A	PGC 12608	7	−16.71	A

Table 1 – *continued*

Name	T type	Abs. 3.6 μm AB mag	Classification	Name	T type	Abs. 3.6 μm AB mag	Classification
PGC 12664	7	−18.91	A	PGC 45195	9	−18.78	A
PGC 12981	9	−17.88	A	PGC 45359	10	−16.22	A
PGC 14487	9	−17.51	A	PGC 45652	99	−19.66	U
PGC 14768	7	−17.63	E	PGC 45958	5	−999	U
PGC 15214	10	−16.34	A	PGC 46261	6	−20.04	C
PGC 15625	10	−17.12	A	PGC 47721	2	−20.48	C
PGC 16389	10	−12.90	U	PGC 48087	5	−19.12	TT?
PGC 16784	8	−18.31	A,TT	PGC 49521	8	−17.11	E
PGC 24469	9	−18.09	A,TT,C	PGC 51291	10	−18.11	E
PGC 28308	−1	−21.72	W?	PGC 52336	99	−999	U
PGC 29086	8	−15.14	E	PGC 52809	7	−19.95	A
PGC 29653	10	−13.73	U	PGC 52935	10	−17.83	I,C
PGC 31979	7	−18.38	E	PGC 52940	9	−18.62	I,C
PGC 35271	10	−14.53	A	PGC 53134	8	−18.82	TT,I,C
PGC 36217	6	−18.94	A	PGC 53634	8	−17.97	E
PGC 36643	7	−18.60	E	PGC 54817	99	−18.87	TT
PGC 37373	7	−18.26	U	PGC 65367	10	−11.25	U
PGC 38250	8	−17.94	U	PGC 66559	8	−18.44	TT,M,C
PGC 41725	9	−16.80	E	PGC 67871	7	−18.21	U
PGC 41965	8	−18.13	A	PGC 68061	4	−19.40	I
PGC 42868	6	−19.30	A	PGC 68771	8	−18.99	E
PGC 43341	9	−17.10	A	PGC 69404	99	−20.94	U
PGC 43458	7	−19.35	A	PGC 69415	10	−14.35	U
PGC 43679	7	−19.39	C	PGC 72006	8	−17.09	E
PGC 43851	10	−16.41	U	PGC 91228	10	−14.25	U
PGC 44278	11	−17.27	U	PGC 91408	8	−16.92	C
PGC 44532	10	−16.96	U	PGC 91413	9	−17.36	A
PGC 44906	9	−17.96	A				

Notes. Classification symbols are A – asymmetry; E – extension; W – warp; TT – tidal tail; S – shell; I – interaction; M – merger; PR – polar ring; C – companion; U – uncertain. 'U' in the Classification column means that any feature detection was very uncertain, often due to a bright star right next to a galaxy or a low surface brightness light distribution that gives the galaxy a very patchy appearance. A question mark (?) after a classification letter means that the classification of that feature as such was uncertain (but not due to an overall uncertainty factor which is marked by the 'U' letter). The morphological 'T'-type is based on classification in the 3.6 μm IRAC images (Buta et al. 2014) and the 3.6 μm absolute AB magnitudes are from Muñoz-Mateos et al. (2014). '99/−999' is used in the second and third columns, respectively, if the value could not be derived from the data, for example if the galaxies are right next to a very bright star, are resolved out (did not have a continuous disc) or have an extremely low surface brightness.

and may be missed in a visual search. We did not use any velocity information in our interaction/merger classifications. Thus, two or more galaxies close to each other in systemic velocity but with no bridge feature between them would be classified as 'companions' (see below). A merger leaves behind a very disturbed morphology and tidal features, but no signs of two (or more) separate galaxy bodies are left over. Kinematic observations of galaxies in our merger class should be able to reveal whether they are truly mergers or just irregular galaxies.

(vii) Polar rings around main galaxy bodies. For definitions, see again Athanassoula & Bosma (1985). Polar rings are features that are usually perpendicular to the position angle of the major axis of the galaxy, but they can exist at other apparent angles as well. They are often needle-like features extending outside the main bodies at a sharp angle to the major axis.

(viii) Companion galaxies. We looked for nearby companion galaxies in the imaged area around the sample galaxies and if found, checked their systemic velocity. If the systemic velocity, checked using the NASA/IPAC Extragalactic Database (NED), was within ±600 km s^{-1} of the target galaxy systemic velocity, we classified it as a companion galaxy. Previous studies using isolation criteria or searches for companion galaxies often use systemic velocity ranges between 500 and 1000 km s^{-1} (e.g. Zaritsky et al. 1993; Sales & Lambas 2005). Our value of 600 km s^{-1} is a compromise between these two, and represents the velocity dispersion of a modest size cluster of galaxies (less than Virgo), and more than that of a galaxy group, so we would find galaxy group members. There can be interacting galaxies beyond this cut in some rare cases, such as possibly NGC 4435 and NGC 4438. Note that the physical size of the imaged area varied a lot, as the sample galaxies are at distances from 1 to about 60 Mpc (almost all of them within about 40 Mpc), and vary in physical size as well. If a velocity measurement was not available for a nearby galaxy, we did not include it as a physical companion galaxy.

In addition to these detected features, we kept track of image features that made the search for these faint outer features associated with the galaxy very uncertain or impossible. Such interfering features include most often bright stars that are located on top of, or near the edges of the main bodies of the galaxies, remaining image artefacts, pointings where the galaxy is near the edge of the field of view, and galaxies with very patchy and faint morphology, showing

no continuous main bodies. All these galaxies are marked with a 'U' in Table 1. Note that '?' in the Classification column in Table 1 after a feature symbol means that the assignment of a feature into one of the abovementioned classes was uncertain, but not due to the interfering feature uncertainty marked by the letter 'U.'

The displayed asymmetries most often have a clear departure from a pure elliptical outer edge. This can in some cases be due to the presence of strong spiral arms that continue outside the main body of the galaxy (e.g. NGC 2750 in Fig. 1). Some galaxies are not elliptical at all in their outer regions, such as NGC 3628 in Fig. 1. More extreme departures from elliptical outer isophotes are also seen.

There may be some overlap between the categories of 'asymmetric' and 'extensions'. However, we considered an extension to be a feature clearly protruding out of the galaxy disc, instead of, for example, a slight extension of one 'side' of the galaxy compared to others. Fig. 2 illustrates what we consider to be extensions. Often the extensions are small-scale features protruding out from the galaxy.

There is possibly some overlap between the 'extension' and 'tidal tail' categories as well. We considered extensions usually to be linear features protruding out of the galaxy discs at close to right angles to the major axis, whereas curved features often seen starting close to the end of the major axis are considered to be tidal tails. The presence of an 'interacting' or 'merger' morphology is a reason to consider an extended feature a tidal tail instead of an extension.

Real warps of the disc are naturally seen only in fairly high inclination galaxies ($i > \sim 65^\circ$; Fig. 5). But as stated earlier, we allowed elongated and twisted irregular galaxies to have 'warps' as well. However, when calculating the statistical numbers of warps, we only counted warps in highly inclined galaxies as explained in detail below.

Polar rings were the hardest features to discern in the images, and they are rare. Image artefacts, such as, for example, the presence of column pull down (examples are seen in the IRAC Instrument Handbook)[1], may conspire to create a polar-ring-like impression. Partly for this reason, our polar ring assignments are all uncertain.

4 THE CATALOGUE, STATISTICS, AND CORRELATIONS OF FEATURES

The main catalogue is presented in Table 1. We list the galaxy name, the 3.6 μm T type (Buta et al. 2010, 2014), the galaxy absolute 3.6 μm AB magnitude (Muñoz-Mateos et al. 2014), and the presence of any detected features. The 17 Hubble types from E to dE/dS/Sph are assigned numerical T values as follows: −5 (E), −4 (E$^+$), −3 (S0$^-$), −2 (S0^0), −1 (S0$^+$), 0 (S0/a), 1 (Sa), 2 (Sab), 3 (Sb), 4 (Sbc), 5 (Sc), 6 (Scd), 7 (Sd), 8 (Sdm), 9 (Sm), 10 (Im), and 11 (dE, dS, or Sph) (de Vaucouleurs & de Vaucouleurs 1964; Binggeli, Sandage & Tammann 1985; Kormendy 2012; Kormendy & Bender 2012). The AB magnitudes were calculated using the mean redshift-independent distance from NED whenever available, and a Hubble constant of 71 km s^{-1} Mpc^{-1} otherwise.

4.1 Asymmetric galaxies and extensions

Asymmetries are by far the most common feature we found. We found 506 asymmetric galaxies in the sample, or 22 ± 1 per cent (uncertainty is purely statistical, calculated as the standard deviation of a binomial distribution). There is of course a large range in the magnitude of asymmetry. Even if we remove the questionable cases, we are left with 469 or 20 ± 1 per cent asymmetric galaxies in a sample of 2352 galaxies. Earlier studies, such as Rix & Zaritsky (1995) who examined a sample of 18 face-on spiral galaxies in the K' band and found that a third of them were lopsided, and Reichard et al. (2008, and see references therein), who inspected over 25 000 galaxies in the Sloan Digital Sky Survey, measured lopsidedness in the whole galaxy disc, although the latter study found that lopsidedness (that causes asymmetry) increases with radius (see also Zaritsky et al. 2013). Our result for the asymmetry fraction can also be compared to the quantitative morphological classification of S^{4}G galaxies inside their luminous bodies by Holwerda et al. (2014). They find that roughly one-quarter of the S^{4}G sample galaxies are 'disturbed', meaning that according to concentration–asymmetry–clumpiness (CAS) criteria (Conselice 2003) these galaxies have an asymmetry value larger than their smoothness value, and the absolute value of the asymmetry is greater than 0.38. Note that the quantitative criterion uses all the pixels inside the $\sim R_{25}$ radius but not outside of it, in the regions that we are concerned with in this paper and thus there may be a detection of asymmetry in the quantitative classification scheme but not in our visual examination which only considered the radii at R_{25} and outside of it. Therefore, the asymmetry fractions in the current paper and in Holwerda et al. (2014) are not directly comparable.

We plot the distributions of absolute 3.6 μm AB magnitudes and T types for asymmetric galaxies in Figs 9 and 10, respectively. As less massive late-type galaxies are structurally more prone to outer disc disturbances than early-type massive elliptical and lenticular galaxies due to the often younger and kinematically more uniform stellar populations of the less massive, late-type galaxies, we expect, and observe, that the fraction of asymmetries goes up towards the later types. Similarly, using quantitative measurements in a small S^{4}G subsample, Zaritsky et al. (2013) found that there is greater lopsidedness for galaxies of later type and lower surface brightness. A similar increase in asymmetry towards later types was seen in the quantitative S^{4}G morphology paper (Holwerda et al. 2014). Also Bridge, Carlberg & Sullivan (2010) found that the least massive galaxies have a higher merger rate and therefore presumably look more asymmetric than the massive galaxies at low redshifts (their sample went down to $z = 0.2$), consistent with our results at z close to zero. The S^{4}G sample is dominated by 'extreme late-type galaxies' (Sd, Sdm, Sm, and Im), and these types are characteristically asymmetric, especially Sdm and Sm. The use of a radio radial velocity in the sample definition weighted the sample towards these types. The luminosity distribution shows that the S^{4}G sample is magnitude limited, and therefore distant, intrinsically faint galaxies are not included.

It is notable that only 14/48 or 29 ± 7 per cent of the galaxies classified as undergoing an interaction in our study have asymmetric outer discs (Table 2). On the other hand, out of the 506 galaxies with asymmetric outer disc classifications in our study, only 14 are interacting galaxies, based on visual bridges between galaxies. This result, combined with the fact that only 64/212 or 30 ± 3 per cent of galaxies that have companions within the mapped area have asymmetric outer discs (Table 2), has been used as evidence by Zaritsky et al. (2013) to argue that small lopsidedness in the S^{4}G sample of galaxies is mainly caused by internal factors, such as dark halo asymmetries. Small asymmetries in the dark halo can give rise to larger, observable stellar asymmetries (Jog & Combes 2009). However, one should keep in mind that our low correlation of

[1] http://irsa.ipac.caltech.edu/data/SPITZER/docs/irac/iracinstrumenthandbook/

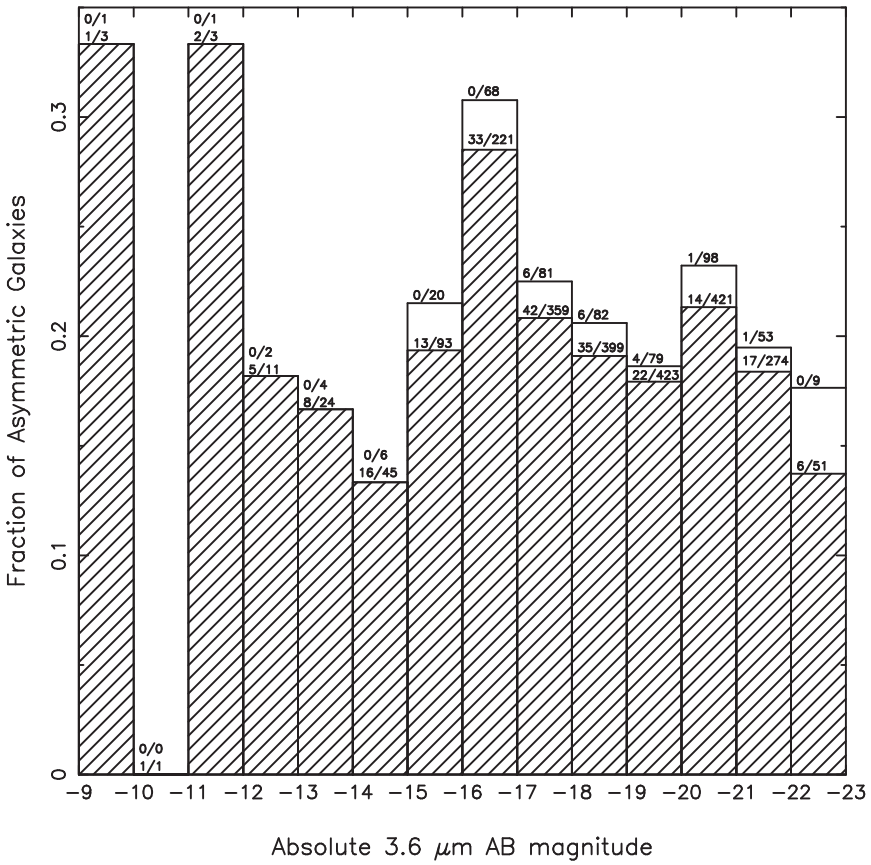

Figure 9. Fraction of asymmetric galaxies as a function of 3.6 μm absolute AB magnitude. The fraction of uncertain (marked by the symbol '?' in Table 1) asymmetries is plotted without hatching. The fractions of (1) asymmetric galaxies in a given magnitude bin with the overall uncertainty flag 'U' in Table 1 over all asymmetric galaxies in the given magnitude bin (see Table 1) and (2) all galaxies in a given magnitude bin with the uncertainty flag 'U' over all galaxies in that magnitude bin are given above the corresponding magnitude column. The luminosity could not be determined for four asymmetric galaxies and 21 galaxies in the whole sample.

asymmetries with interactions and companions may be caused by (1) the outer isophotes remaining relatively elliptical even if there is a minor perturbation (satellite interaction or minor merger); (2) not being able to count all the companions because of limitations in the field of view and depth of the survey; and (3) as compared to such samples as the Galaxy Zoo (Casteels et al. 2013), our sample size being still relatively small.

There may be several different origins for the outer disc asymmetries, including internal effects, such as lopsidedness (Zaritsky et al. 2013). If we assume that they are overwhelmingly due to interactions, it is possible to make an argument for the duration of asymmetries in outer discs due to interactions as follows. The magnitude of the brightness asymmetries in the outer halves of the discs of several galaxies studied here is around 50 per cent. We estimate whether this is high enough to produce significant torques and radial flows if the disc mass follows the disc light. We consider for simplicity a 180° asymmetry of magnitude $A \sim 50$ per cent. Then the outer disc mass in four quadrants varies in azimuth as $M_4(1 - A/2)$, M_4, $M_4(1 + A/2)$, and M_4, where M_4 is one-quarter of the disc mass in the radial interval of the asymmetry, say, the outer half of the disc. In this case, the forward and backward torques on the minor axes of the asymmetry are

$$\text{Torque} = GM_4M_4[(1 + A/2) - (1 - A/2)]R/(1.4R)^2, \quad (1)$$

where R is the average radius of the outer disc and $2^{0.5}R \simeq 1.4R$ is the distance between quadrants in the outer disc where the masses are M_4 and $M_4(1 \pm A/2)$.

Setting the torque on a quadrant equal to the time derivative of M_4RV (where V is the rotation speed and R is the radius), and considering that the mass and rotation speed do not change much during the subsequent adjustment, we obtain the radial outflow or inflow speed V_R that is driven by this asymmetry:

$$V_R/V = \frac{AM_{\text{outer disc}}}{8M_{\text{gal}}}, \quad (2)$$

where $M_{\text{outer disc}} = 4M_4$ is the total disc mass in the radial range of the asymmetry and M_{gal} is the total galaxy mass inside the radius R that gives the rotation speed, using the equation $V^2 = GM_{\text{gal}}/R$.

If we consider that the outer disc mass is ∼10 per cent of the total mass inside the radius R, then $V_R/V \sim 0.012A$, which is a fairly small effect at any one time, giving e.g. $V_R \sim 1$ km s^{-1}. This is barely enough to relax and mix an outer asymmetry spanning a radial range of ∼10 kpc by disc torques in a Hubble time.

More important would be mixing and smearing of the asymmetry by shear given the rotation curve from dark matter. In the outer disc, the rotation time is $2\pi R/V \sim 0.5$ Gyr, so this would be the approximate lifetime of an initially 180° asymmetry at $R \sim 20$ kpc before shear turns it into a spiral or tidal arm. Galaxy interactions

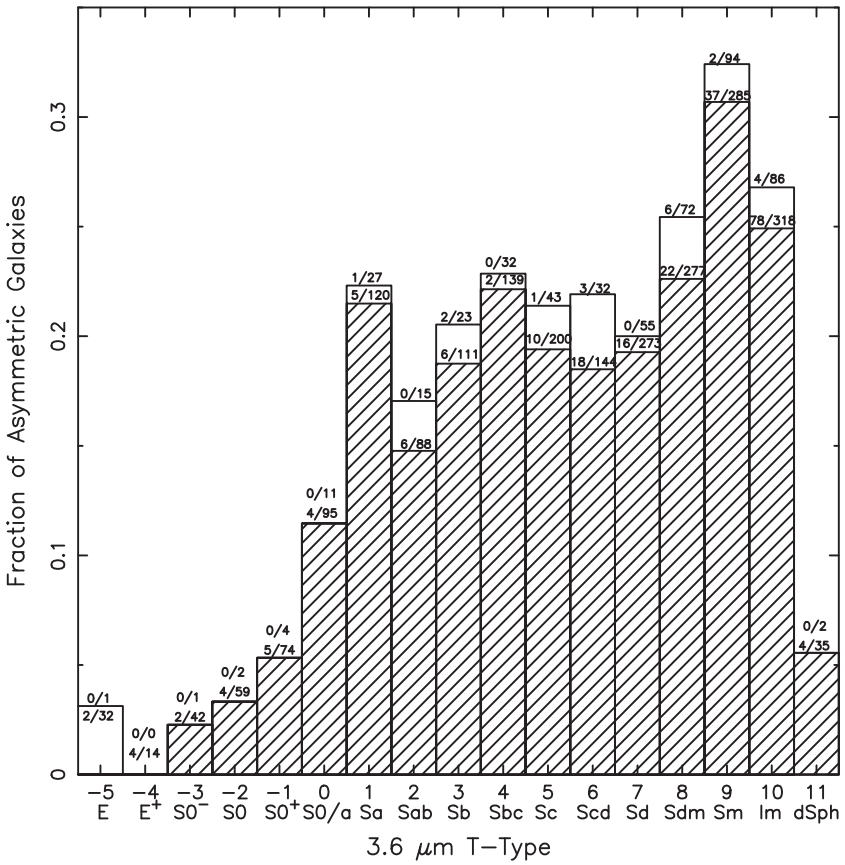

Figure 10. Fraction of asymmetric galaxies as a function of 3.6 μm T type. The fraction of uncertain (marked by the symbol '?' in Table 1) asymmetry detections are plotted without hatching. The fraction of asymmetric galaxies in a given T-type bin with the overall uncertainty flag 'U' in Table 1 over all asymmetric galaxies in that T-type bin (see Table 1) and the fraction of all galaxies in a given T-type bin with the uncertainty flag 'U' are given above the corresponding T-type column. The T type could not be determined for six asymmetric galaxies and 18 galaxies in the whole sample. The 'dSph' type includes dE, dS, and Sph types.

Table 2. Main outer region statistics of S^{4}G galaxies.

Asym.	Unq. Asym.	Asym. Int.	Asym. Comp.	Ext.	Warps
22 ± 1 per cent	± 1 per cent	29 ± 7 per cent	30 ± 3 per cent	6 ± 1 per cent	7 ± 1 per cent (12 ± 4 per cent)

Notes. Unq. = unquestionable; Asym. = asymmetries; Int. = interacting; Comp. = companions; Ext. = extensions. Warp fractions are for galaxies with incl. >65° (>80°). The third and fourth columns give the fraction of asymmetric galaxies among interacting galaxies and among galaxies with companions, respectively.

that perturb discs down to $R \sim 5$ kpc would produce tidal arms four times faster, in ∼0.1 Gyr.

However, asymmetries in the far outer disc might still be visible after several rotations, or some ∼4 Gyr, as suggested by the cosmological zoom re-simulations in Section 5. If only half the galaxies have a strong interaction which leaves signs that last for 4 Gyr, then in 10 Gyr (a typical galaxy age) we would see 40 per cent of that half with an outer disc asymmetry, or a total of 20 per cent of all galaxies that we see at any given time would have an asymmetry, assuming that interactions take place at random times during the 10 Gyr galaxy age. This 20 per cent is comparable to the fraction of discs in our survey that have perceptible outer disc asymmetries, suggesting that many of these structures could be remnants of interactions less than about ∼4 Gyr ago, with the older structures now mixed and invisible. It should be noted that the lifetime estimates we get this way depend on the assumption that the asymmetries are exclusively due to interactions. If other factors are in play, the lifetime of the features could be shorter or there may have been fewer interactions.

It is also interesting to compare our estimate of about 20 per cent asymmetries to the fractional estimate of 15 per cent of asymmetric, lopsided, warped, or distorted with an integral-sign-like appearance or tidal feature (tail, bridge, or shells) in the sample of Fernández Lorenzo et al. (2012) of visible light images of 466 isolated nearby galaxies with systemic velocities between 1500 and 24 000 km s^{-1}. This difference may be due to different depths of the surveys, different distance limits on the samples, and a different wavelength region surveyed.

Extensions were found in 6 ± 1 per cent of the whole S^{4}G sample. Figs 11 and 12 display histograms versus 3.6 μm absolute AB magnitudes and T types for galaxies with extensions. We did not find any clear absolute magnitude (more extensions might be expected

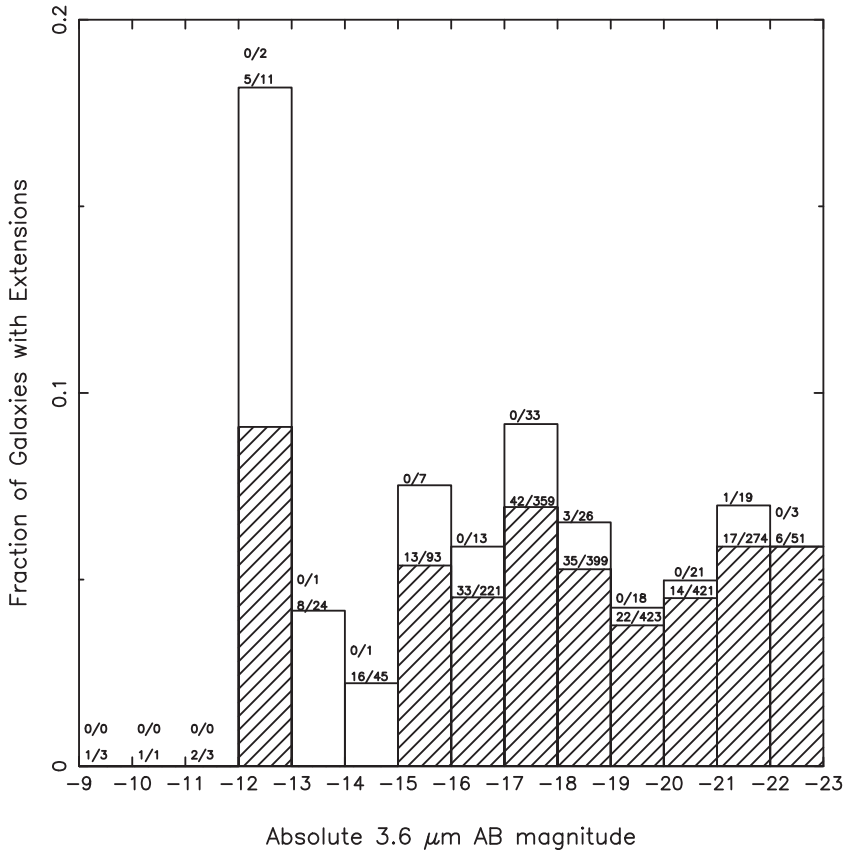

Figure 11. Fraction of galaxies with extensions as a function of 3.6 μm absolute AB magnitude. The fraction of uncertain (marked by the symbol '?' in Table 1) extension detections are plotted without hatching. The fractions of galaxies with extensions in a given magnitude bin with the overall uncertainty flag 'U' in Table 1 over all the galaxies with extensions in the given magnitude bin (see Table 1) and the fraction of all galaxies in a given magnitude bin with the uncertainty flag 'U' are given above the corresponding magnitude column. The luminosity could not be determined for one galaxy with an extension and 21 galaxies in the whole sample.

to be seen among the low mass, often irregular low-luminosity systems) or T-type dependence for extensions.

4.2 Warped galaxies

We have found warps or possible warps in 32 edge-on galaxies among the 489 highly inclined ($i > 65^\circ$) galaxies (7 ± 1 per cent) (see also Comerón et al. 2011). It is likely that the inclination has to be higher than $\simeq 80^\circ$ (e.g. Reshetnikov & Combes 1998) for a warp to become visible in visual or near-IR observations, but we allow here for 'warps' in less inclined galaxies. Using 80° as the minimum inclination, we find warps in nine out of 75 galaxies (12 ± 4 per cent). Warps have been conventionally found in H I observations, e.g. Bosma (1991), where they are often more obvious and produce higher warped fractions in the smaller samples that were observed than here. Warp studies using visible light images detected a higher fraction of warps in the samples that were biased towards more inclined, bright, late-type galaxies, e.g. Sánchez-Saavedra et al. (2003, 53 per cent) and Reshetnikov & Combes (1998, 1999, 40 per cent). The warped galaxies in our study are predominantly less bright than L^*, and have mostly Hubble T types from 3 to 10 (or Sb to Im). We thus confirm the Reshetnikov & Combes (1998, 1999) result concerning galaxy type, but we disagree with the effect of luminosities and so, presumably mass. We have classified 10 other galaxies as warped because our classification took place without a priori knowledge of the inclination of the galaxies. These are mostly galaxies with low inclinations and elongated morphologies and therefore are not 'warped' in the sense of edge-on discs. For four of them, the warp detection is questionable.

4.3 Tidal tails and interactions

Tidal tails are found in 71/2352 galaxies or in 3 ± 1 per cent of the sample galaxies. 24 of these detections are uncertain. Because of the limited map size, it is not clear in many cases which galaxy is causing these tidal features. Several examples of the 'diffuse' tidal tail morphology are seen [in the similar visual classification scheme of Elmegreen et al. 2007 who used it for intermediate-redshift galaxies out to $z = 1.4$ in the Galaxy Evolution from Morphology and SEDs (GEMS) and Great Observatories Origins Deep Survey (GOODS) fields]. Also some examples of the 'antenna' morphology are seen. Our sample can be used as a nearby comparison sample for future comparisons of detections of tidal features in higher z galaxies.

We have recognized 31 interacting systems in the full S^{4}G sample used here. These contain examples of the 'M51-type' and 'shrimp' galaxies as classified by Elmegreen et al. (2007). Equal mass interactions are also represented. However, probably none of our interactions would be classified as 'assembling' in the classification scheme of Elmegreen et al. (2007). This is consistent with the common picture of galaxy evolution where the galaxy assembly took place at high redshifts. However, among the 10 merger systems in the S^{4}G sample there are a few which could be classified as

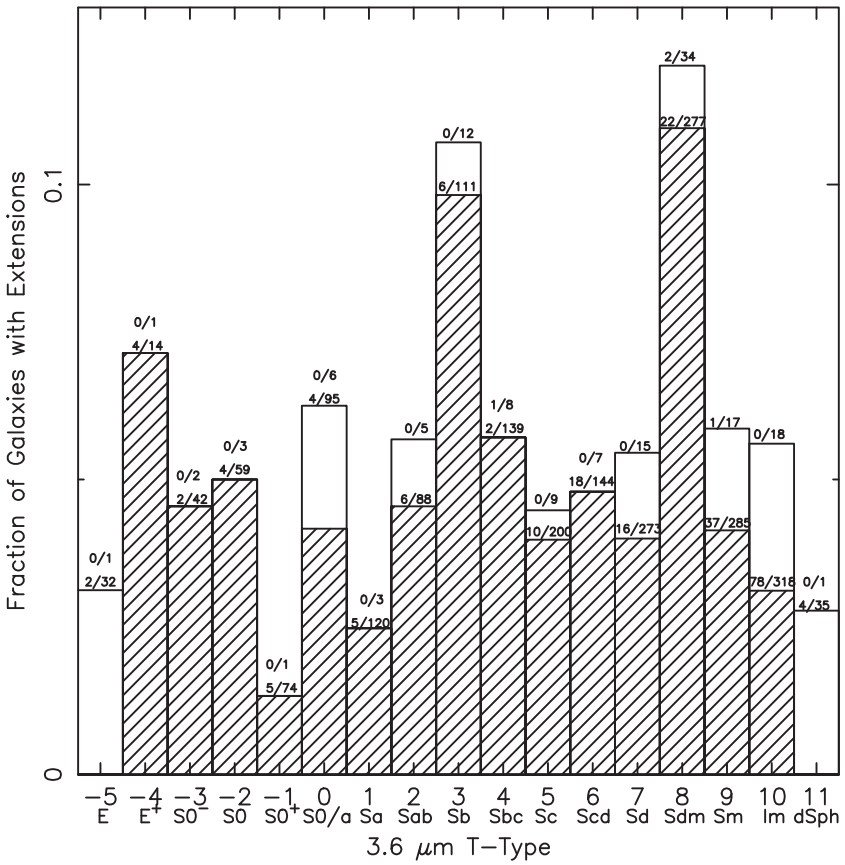

Figure 12. Fraction of galaxies with extensions as a function of 3.6 μm T type. The fraction of uncertain (marked by the symbol '?' in Table 1) extension detections are plotted without hatching. The fraction of galaxies with extensions in a given T-type bin with the overall uncertainty flag 'U' in Table 1 over all the galaxies with extensions in the given T-type bin (see Table 1) and the fraction of all galaxies in a given T-type bin with the uncertainty flag 'U' are given above the corresponding T-type column. The T type could not be determined for two galaxies with extensions and 18 galaxies in the whole sample. The 'dSph' type includes dE, dS, and Sph types.

'assembling' (Fig. 7; NGC 337, NGC 1487). Our complete sample of nearby galaxies should again be useful in future studies that want to compare the frequency of galaxy assembly at higher redshifts to the current epoch (assuming the same rest wavelength, *James Webb Space Telescope* (*JWST*) Mid-Infrared Instrument (MIRI) sensitivity should be sufficient to detect similarly bright features out to a z of about 0.3–0.4 and future detectors may be able to push this limit into even higher redshifts where most of the galaxy assembly took place).

Interactions and mergers were also searched for in visible light images in a parallel project (Knapen et al. 2014). Only 69 per cent of the interactions/mergers in our sample are classified as such in the visible light images. The difference can be explained by different classification criteria used, and the larger imaged areas in the visible light images.

4.4 Shell galaxies

All but one of the eight shell galaxies have T types from 0 to 4, i.e. S0/a to Sbc, thus somewhat surprisingly containing only one elliptical galaxy. This is likely to be due to the small number of elliptical galaxies in the S^{4}G sample (only 46 galaxies of T type −4 or less in the sample due to the selection of S^{4}G galaxies by requiring a radio, most often H I, line heliocentric radial velocity). On the other hand, the possible existence of shell-like features in galaxies as late type as Sbc is interesting. The Sbc galaxy that has shells in the sample, NGC 3310, is a well-known minor merger galaxy and its shells are known (Wehner et al. 2006). The shells of NGC 474, NGC 2782, NGC 3619, and NGC 5218 are also well known. To our knowledge, shells have not been seen in the two questionable cases, IC 3102 and NGC 7727. In the case of NGC 2782, the shells are assumed to be associated with a recent minor merger (e.g. Jogee, Kenney & Smith 1998). NGC 2681 is a multiple ring galaxy (Buta et al. 1994) and the rings may have been mistaken as shells. The shell galaxies in the sample have $M_{3.6}$ values of −20.6 to −21.9, which correspond to less luminous than L^* galaxies. Comparing to the results of Kim et al. (2012), we note that NGC 2634 is not officially part of the S^{4}G sample, and therefore was not examined by us. In NGC 3032 the shell structure is very faint and not visible without doing a deeper analysis involving subtraction of the smooth light, which we did not do (most features of the outer region are visible in the non-smoothed versions of the image, as we paid attention mostly to areas outside the easily visible galaxy discs or spheroids). Similarly, images of NGC 5018 require unsharp masking for the shell features to become clearly visible within the luminous body of the galaxy.

4.5 Polar ring galaxies

Only three polar ring candidate galaxies were detected among the S^{4}G sample galaxies. Of these, NGC 660 (e.g. van Driel et al. 1995) and NGC 5122 (e.g. Reshetnikov, Faúndez-Abans &

de Oliveira-Abans 2001) are known to be polar ring galaxies, while NGC 681 is not known to be a polar ring galaxy. The detection of a polar ring in this galaxy is uncertain due to the thin and large disc that dissects the luminous halo of this galaxy. Even an image where the underlying disc/bulge component has been subtracted, cannot reveal with certainty whether this feature is a ring in the galaxy plane or a polar ring. On the other hand, it is interesting that the well-known polar ring galaxy NGC 2685 was not detected in the S^{4}G 3.6 μm image. This is likely so because the polar ring is actually within the main body of the galaxy when looking at it with the histogram equalization scale in DS9. It only shows up as a loop-like feature with the logarithmic intensity scale. Polar rings are also less obvious in the older stellar population revealed at 3.6 μm. There are probably other polar rings in the sample at unfavourable orientations and thus they were not detected. The loopy features in NGC 5134 are probably part of an outer ring (Buta & Crocker 1991, 1992). Also, based on the findings of Schweizer, Whitmore & Rubin (1983) we would have expected to find more than one polar ring among the S0 galaxies as Schweizer et al. (1983) found a few per cent of all field S0 galaxies to have polar rings.

Other polar rings have been found in the S^{4}G sample galaxies NGC 2748, NGC 6870, and NGC 7465, by Buta et al. (2014). Their tentative contours are marked in the appendices of Comerón et al. (2014). However, those three polar rings are exceedingly subtle and/or hard to interpret. Therefore, they may actually not be polar rings. This is the position adopted in this paper.

4.6 Companion galaxies

In addition to the outer features, we also checked for nearby companions that were visible in the 3.6 μm images (usually within about 10 arcmin of the sample galaxies) by checking for their systemic velocities in NED. A galaxy was called a companion if it was within ±600 km s^{-1} of the sample galaxy in systemic velocity. Because the images cover an arbitrary extent of space, and more in some directions than in others, some companion galaxies were missed in these images. We also present statistics of detected and confirmed companion galaxies versus the 3.6 μm luminosity and the T type in Figs 13 and 14, respectively. Companions appear to be found most frequently around galaxies with absolute 3.6 μm AB magnitudes around −22 to −24, possibly because they are the brightest galaxies in the sample and thus are expected to have the brightest companions that are easy to detect, and T types around −4 and 2, corresponding to Hubble classes E$^+$ and Sab.

Companions have also been searched for in visible light images of S^{4}G galaxies (Knapen et al. 2014). However, the companion definition criteria were different. For example, the velocity difference between the companion and the host galaxy was constrained to be less than ±200 km s^{-1} in the visible light-based search. In addition, the search area was more limited in the 3.6 μm images, the 3.6 μm companion selection includes uncertain cases, and the visible light sample includes 477 more galaxies, so the two samples

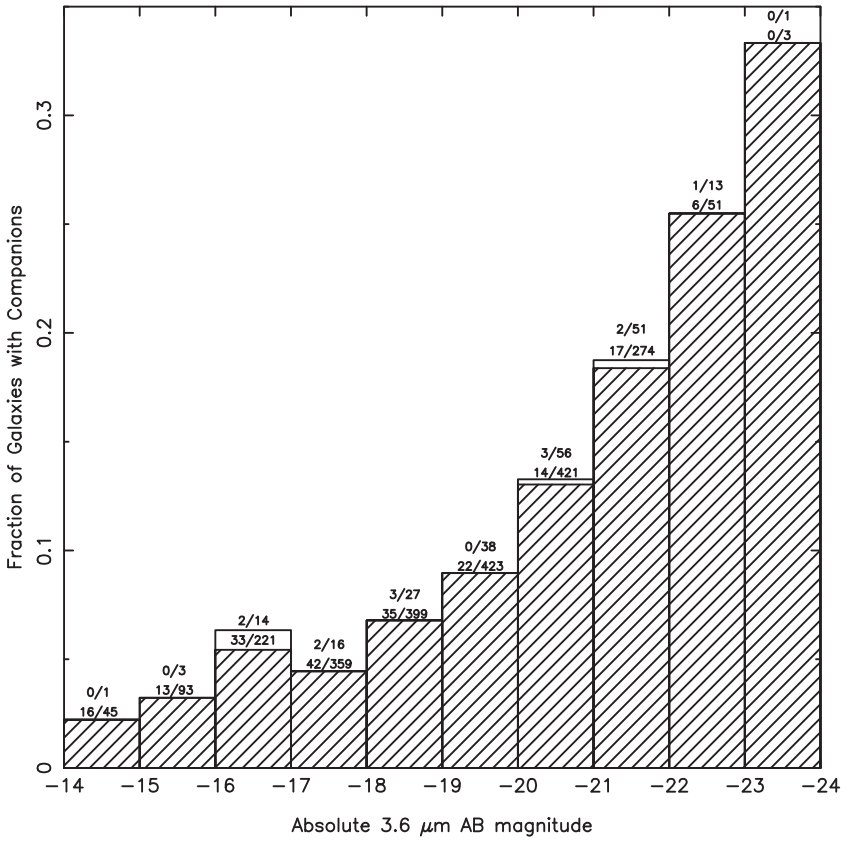

Figure 13. Fraction of galaxies with companions as a function of 3.6 μm absolute AB magnitude. The fraction of uncertain (marked by the symbol '?' in Table 1) companion detections is plotted without hatching. The fractions of galaxies with companions in a given magnitude bin with the overall uncertainty flag 'U' in Table 1 over all the galaxies with companions in the given magnitude bin (see Table 1) and of all galaxies in a given magnitude bin with the uncertainty flag 'U' are given above the corresponding magnitude column. The luminosity could not be determined for two galaxies with companions and 21 galaxies in the whole sample.

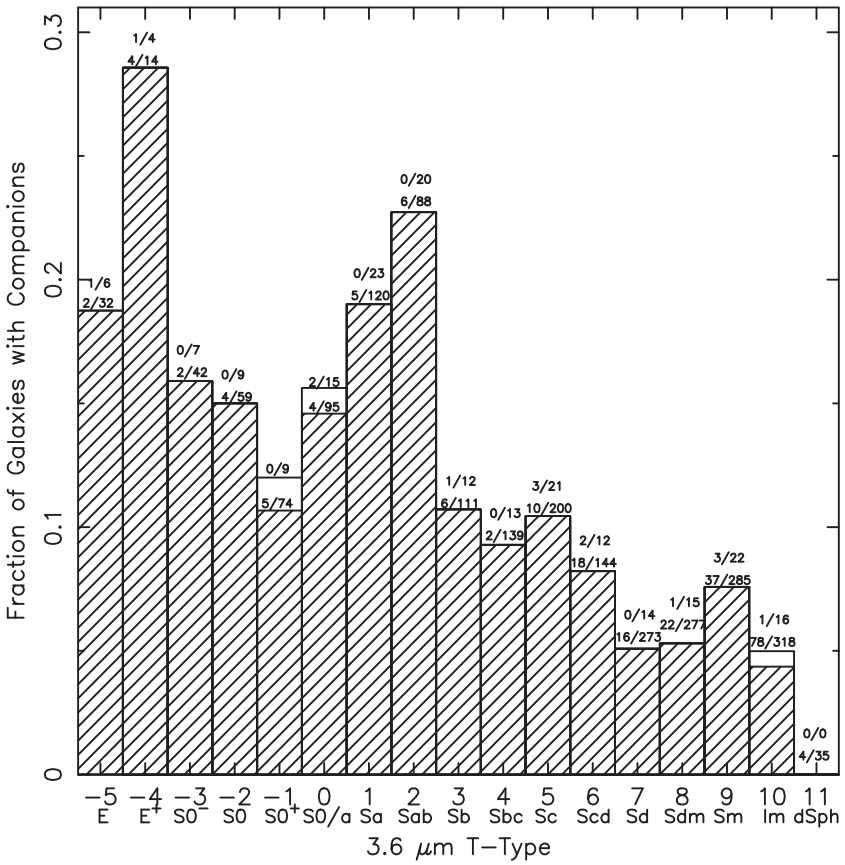

Figure 14. Fraction of galaxies with companions as a function of 3.6 μm T type. The fraction of uncertain (marked by the symbol '?' in Table 1) companion detections are plotted without hatching. The fraction of galaxies with companions in a given T-type bin with the overall uncertainty flag 'U' in Table 1 over all the galaxies with companions in the given T-type bin (see Table 1) and the fraction of all galaxies in a given T-type bin with the uncertainty flag 'U' are given above the corresponding T-type column. The T type could not be determined for four galaxies with companions and 18 galaxies in the whole sample. The 'dSph' type includes dE, dS, and Sph types.

are not comparable (only 64 per cent of the S^{4}G galaxies that we classified as potentially having companions in the 3.6 μm images are listed as having companions in the visible light images). It is difficult to draw any definite conclusions regarding the existence of companions in the S^{4}G images, partly because of the limitations of the depth, coverage, and size of the sample.

4.7 Comparison to faint features seen at other wavelengths

We estimate that in our survey we pick up in several cases faint features not readily seen in standard shallow visible light images. Targeted deep optical imaging may go deeper in several other cases. For example, we do not detect the faint loops around NGC 4013 (Martínez-Delgado et al. 2009) and NGC 5907 (Martínez-Delgado et al. 2008), partly because the field of view (FOV) of our IRAC observations is not large enough. For other galaxies, such as the eight galaxies with very faint optical features discussed in Martínez-Delgado et al. (2010), who used an uncalibrated luminance filter covering most of the visible light wavelength regime, the score is mixed. For some of the galaxies again the FOV is relatively small (e.g. NGC 3521 and NGC 5055), while for others a few red faint features are detected (e.g. the companion of NGC 7531 already discussed in Buta 1987, and the extensions of NGC 4651), while for yet others we miss some of the outer features readily seen in *Galaxy Evolution Explorer* (*GALEX*) data, which must hence be composed of young stellar populations without counterparts in the near-IR (e.g. the outer disc of NGC 7531 itself).

5 SIMULATION COMPARISON

We have made the first attempt to utilize the information from the detected faint outer region features to constrain the evolution of galaxies over their lifetimes. We do this by comparing the outer region features in the 3.6 μm images to similar features around galaxies in zoom re-simulations of cosmological galaxy evolution simulations. We have analysed a sample of 33 simulated galaxies from Martig et al. (2012). In that work each galaxy was simulated with a zoom re-simulation technique described in detail in Martig et al. (2009). Star formation followed a Schmidt law with an exponent of 1.5 (above a gas density threshold of 0.03 $M_\odot$ pc^{-3}). Martig et al. (2012) also took into account kinetic supernova feedback and mass loss from evolved stars. The exact star formation and feedback prescriptions probably affect the location and magnitude of outer disc asymmetries. We are still missing substantial physics and numerical resolution to fully model realistic galaxies. The spatial physical resolution was 150 pc, and the mass resolution 1.5×10^4 $M_\odot$ for gas and star particles, and 3×10^5 for dark matter particles.

The 33 simulated haloes from Martig et al. (2012) are a large set of high-resolution zoom re-simulations, with various galaxy

formation histories that give rise to various morphologies during their evolution that is followed to $z = 0$, and therefore they form a good set for a comparison between observed features and those forming in simulations. The simulated galaxies were selected to have a mass between 2.7×10^{11} and 2×10^{12} $M_\odot$ at $z = 0$, and as being in an isolated environment at $z = 0$. They have a wide range of formation histories, from galaxies with recent major mergers to galaxies with no merger with a mass ratio greater than 1:10 in the last 9 Gyr. This resulted in a wide range of morphologies at $z = 0$, even if 85 per cent of the sample has a bulge-to-total stellar mass ratio smaller than 0.5 (see Martig et al. 2012). Their final stellar mass ranges from 1.7×10^{10} to 2×10^{11} $M_\odot$.

To compare these simulated galaxies from Martig et al. (2012) to S^{4}G data, we computed mock 3.6 μm images for all 33 galaxies, at seven inclinations ranging from 0° to 90°. The mock 3.6 μm images were computed using the PEGASE.2 stellar evolution code (Fioc & Rocca-Volmerange 1999), assuming a Kroupa initial mass function from 0.1 to 120 $M_\odot$ (we did not include any dust contribution because at 3.6 μm dust is not expected to play a significant role and can be excluded in the modelling). Each image corresponds to 100×100 kpc^2 in size (with a similar total depth of 100 kpc). Each pixel represents 143×143 pc^2, which in terms of IRAC pixels corresponds to a galaxy situated 24 Mpc away (the S^{4}G sample galaxies are at distances of 1–60 Mpc, although almost all of them are within 40 Mpc). We added an expected background of 0.15 MJy sr^{-1} which corresponds to a medium background level in IRAC images. We then converted the image into mock IRAC 30-s frames in electron units. Next we generated a Poisson variate for the flux value from IDL's RANDOMU function, and added in the read noise contribution which is 14.6 electrons. We then added noise to an artificial sky dark, using a typical median value of 0.05 MJy sr^{-1} or 38 electrons, and subtracted it from the noise-added galaxy image. Finally, we converted the image to MJy sr^{-1}, and made eight realizations of these images, corresponding to the IRAC observing depth, and took the median of them to form the final image. We selected each of the 33 simulated galaxies in a random order but with such inclinations that the observed S^{4}G inclination distribution was reproduced. We then classified the inclined galaxy mock images in exactly the same way as we classified the S^{4}G IRAC channel 1 images.

The detected outer disc features in the simulated galaxies are shown in Figs 15 and 16. We have looked at the time series of simulations. It is often not obvious what the causes of the outer disc asymmetries or extensions are, but probable culprits include ongoing interactions, asymmetric spiral structure resulting from a simple companion galaxy fly-by 2–4 Gyr ago (comparable to the age estimate of visible interaction signs from abnormal colours or fine structure by Schweizer & Seitzer 1992; however, it should be noted that such a flyby does not always result in detected asymmetric structure), 'chaotic' disc reformation after a recent merger (the old disc was destroyed by the merger, and a new disc is still in the process of settling down and therefore it appears asymmetric or has extensions), and long-lived (5 Gyr or more) asymmetric spiral structure (this may be related to asymmetries in external gas accretion). The best way forward is to statistically compare large samples of observed and model galaxies to explore a range of possible origins. Future models may also provide other clues to the origin of these features, such as colours, clumpiness measurements, etc.

We find asymmetric outer discs in 11/33 galaxies or 33 ± 8 per cent, and we find a similar fraction of outer disc extensions (33 per cent). These numbers are higher than the fractions of outer disc asymmetries and extensions in the S^{4}G sample. Possible reasons

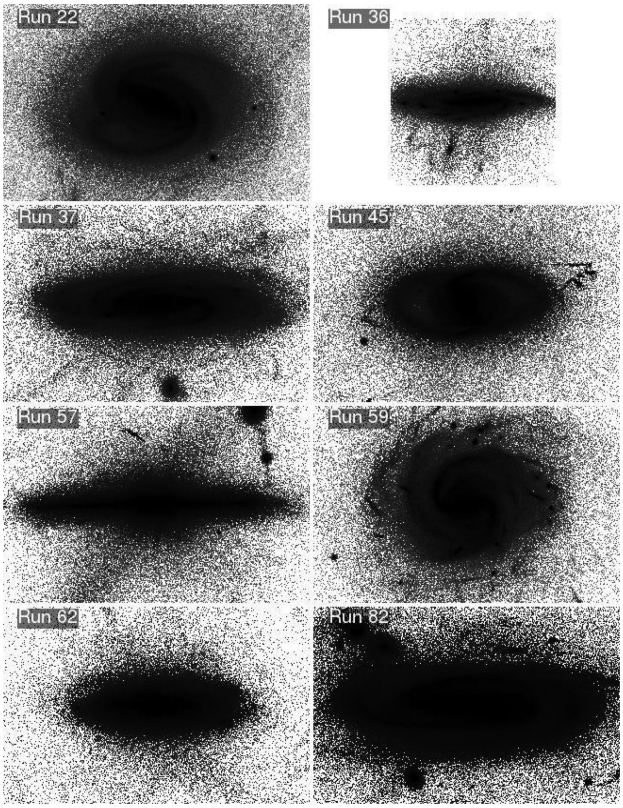

Figure 15. Images of outer disc asymmetries in simulated galaxies. Images of all the detected asymmetries are available in the online version of the journal.

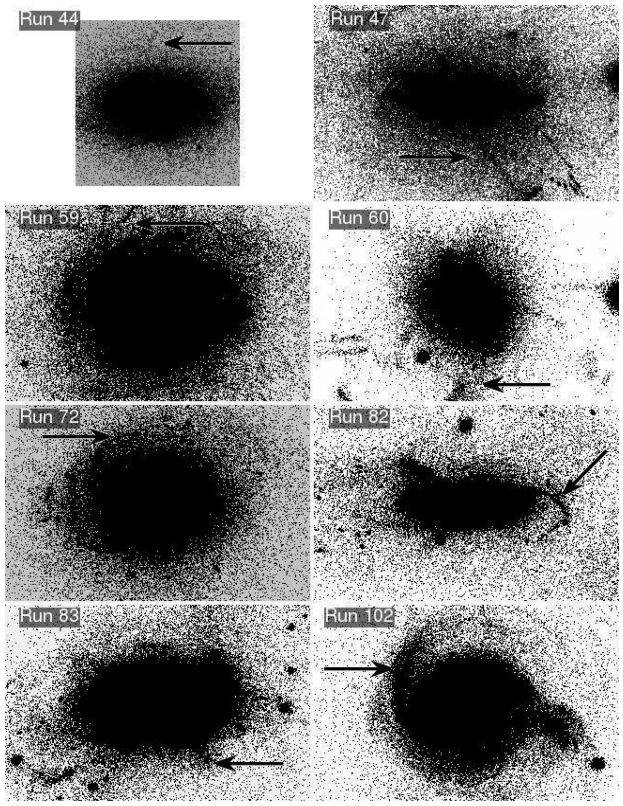

Figure 16. Images of outer disc extensions in simulated galaxies. Images of all the detected extensions are available in the online version of the journal.

for this discrepancy include the fact that the simulation sample consists of mostly late-type disc galaxies, whereas the S^{4}G sample has several earlier type galaxies. As seen in Fig. 10, asymmetries are more prevalent (around 25 per cent) among late-type disc galaxies than in the S^{4}G sample as a whole. Also, our current inability to model the physics of star formation is likely to affect details of asymmetry formation. For example, if the star formation gas density threshold used in the simulations was higher, then the visible disc would be detected to smaller radii where the galaxy is more symmetric. Therefore, the simulated galaxies may allow star formation further out than real galaxies. Put another way, the fraction of asymmetries in the outer regions of real galaxies may be 33 per cent, but without star formation in the outer parts, a fraction of the asymmetries would not be visible. Also, outer discs may have an additional condition for star formation, other than a critical density, such as needing to form molecules at low metallicity. In fact, anything that makes a real galaxy less able to form stars in the far outer part than the simulated galaxy would seem to lower the asymmetry fraction for real galaxies.

The reason for the high fraction of extensions in the simulated sample is less clear, but it could mean that some parameters in the simulations require further adjustments to make the simulated galaxies look more realistic as a whole. We found a companion and an interaction in only one of the 33 galaxies (this is partly a selection effect because the simulated galaxies were selected to be isolated at $z = 0$).

6 CONCLUSIONS

This paper presents discoveries and classifications of near-IR-detected stellar features outside the main bodies of galaxies (at and outside of R_{25}) in the complete sample of 2352 S^{4}G galaxies. The detected features include asymmetries, extensions, polar rings, warps, shells, tidal tails, and interaction/merger morphologies. We also tabulate nearby companion galaxies, confirmed by a reasonable systemic velocity difference of ± 600 km s^{-1} in NED, as seen in the 3.6 μm images. This list of outer disc features is conceived to be an important data base for future quantitative studies of them when higher S/N observations become available.

We also give statistics on the features we detected. The fraction of asymmetric galaxies in the S^{4}G sample is about 20 per cent. If the ∼20 per cent fraction of galaxies with asymmetries in their outer discs is overwhelmingly due to interactions, it may imply that half of all galaxies have interactions that leave visible signs for ∼4 Gyr after the beginning of the interaction. However, an internal origin for some of these asymmetries is also possible, e.g. due to dark halo asymmetry induced lopsidedness. We found that the number of asymmetric galaxies increases with T type, peaking in late Hubble types (T types 5–10), as would be expected, because the later type galaxies are more susceptible to disturbances due to their kinematics and stellar distributions. Surprisingly, we find shells in galaxies of fairly late T types, although shells are commonly believed to be primarily features of early-type galaxies.

In a first attempt to utilize our faint outer feature detections to constrain galaxy evolution on billions of years time-scale, we have also classified galaxies in cosmological zoom re-simulations as seen at $z = 0$, and converted to IRAC-like images. We find a larger outer disc asymmetry fraction (by a factor of 1.5) in the simulated galaxy sample than in S^{4}G, which may be due to selection effects and our incomplete understanding of star formation thresholds. The simulations suggest interactions and mergers, asymmetric external gas accretion, unfinished disc reformation, and asymmetric spiral structure as causes for asymmetry. However, it is difficult to quantify the relative importance of these effects. Finally, the simulations suggest that asymmetries may be visible for at least 4 Gyr after an interaction or merger.

ACKNOWLEDGEMENTS

We thank Ramin Skibba for helpful comments on a draft of this paper. We also thank Carrie Bridge for discussions on the merger rate. We acknowledge the helpful discussion with Chris Lintott about biases in classification. We acknowledge financial support to the DAGAL network from the People Programme (Marie Curie Actions) of the European Union's Seventh Framework Programme FP7/2007-2013/ under REA grant agreement number PITN-GA-2011-289313. This work was cofunded under the Marie Curie Actions of the European Commission (FP7-COFUND). We also gratefully acknowledge support from NASA JPL/*Spitzer* grant RSA 1374189 provided for the S^{4}G project. EA and AB thank the CNES for support. KS, J-C M-M, TK, and TM acknowledge support from the National Radio Astronomy Observatory, which is a facility of the National Science Foundation operated under cooperative agreement by Associated Universities, Inc. The authors thank the entire S^{4}G team for their efforts in this project. This work is based on observations made with the *Spitzer Space Telescope*, which is operated by the Jet Propulsion Laboratory, California Institute of Technology under a contract with NASA. Support for this work was provided by NASA through an award issued by JPL/Caltech. We are grateful to the dedicated staff at the *Spitzer* Science Center for their help and support in planning and execution of this Exploration Science program. This research has made use of the NASA/IPAC Extragalactic Database (NED) which is operated by JPL, Caltech, under contract with NASA.

REFERENCES

Abraham R. G., Merrifield M. R., 2000, AJ, 120, 2835
Abraham R. G., van den Bergh S., Nair P., 2003, ApJ, 588, 218
Adams S. M., Zaritsky D., Sand D. J., Graham M. L., Bildfell C., Hoekstra H., Pritchet C., 2012, AJ, 144, 128
Ade P. A. R. et al., 2014, A&A, preprint (arXiv:1303.5076)
Arp H., 1966, ApJS, 14, 1
Athanassoula E., Bosma A., 1985, ARA&A, 23, 147
Atkinson A. M., Abraham R. G., Ferguson A. M. N., 2013, ApJ, 765, 28
Ball N. M., Loveday J., Fukugita M., Nakamura O., Okamura S., Brinkmann J., Brunner R. J., 2004, MNRAS, 348, 1038
Ball N. M., Brunner R. J., Myers A. D., Strand N. E., Alberts S. L., Tcheng D., 2008, ApJ, 683, 12
Bershady M. A., Jangren A., Conselice C. J., 2000, AJ, 119, 2645
Binggeli B., Sandage A., Tammann G. A., 1985, AJ, 90, 1681
Bosma A., 1991, in Casertano S., Sackett P. D., Briggs F. H., eds, Warped Disks and Inclined Rings Around Galaxies. Cambridge Univ. Press, Cambridge, p. 181
Bournaud F., Combes F., 2003, A&A, 401, 817
Bridge C. R., Carlberg R. G., Sullivan M., 2010, ApJ, 709, 1067
Brook C. B., Governato F., Quinn T., Wadsley J., Brooks A. M., Willman B., Stilp A., Jonsson P., 2008, ApJ, 689, 678
Buta R., 1987, ApJS, 64, 1
Buta R., 1995, ApJS, 96, 39
Buta R. J., 2013, in Oswalt T. D., Keel W. C., eds, Planets, Stars and Stellar Systems. Springer-Verlag, Dordrecht, p. 1
Buta R., Crocker D. A., 1991, AJ, 102, 1715
Buta R., Crocker D. A., 1992, AJ, 103, 1804
Buta R., Mitra S., de Vaucouleurs G., Corwin H. G., Jr, 1994, AJ, 107, 118

Buta R. J., Corwin H. G., Odewahn S. C., 2007, The de Vaucouleurs Atlas of Galaxies. Cambridge Univ. Press, Cambridge
Buta R. J. et al., 2010, ApJS, 190, 147
Buta R. J. et al., 2014, ApJS, submitted
Casteels K. R. V. et al., 2013, MNRAS, 429, 1051
Cheng J. Y., Faber S. M., Simard L., Graves G. J., Lopez E. D., Yan R., Cooper M. C., 2011, MNRAS, 412, 727
Comerón S. et al., 2011, ApJ, 741, 28
Comerón S. et al., 2012, ApJ, 759, 98
Comerón S. et al., 2014, A&A, 562, A121
Conselice C. J., 2003, ApJS, 147, 1
Dale D. A. et al., 2009, ApJ, 703, 517
de Vaucouleurs G., de Vaucouleurs A., 1964, Reference Catalog of Bright Galaxies. University of Texas Monographs in Astronomy, No. 1. Univ. Texas Press, Austin, TX
Elmegreen D. M., Elmegreen B. G., Ferguson T., Mullan B., 2007, ApJ, 663, 734
Eskew M., Zaritsky D., Meidt S., 2012, AJ, 143, 139
Fazio G. G. et al., 2004, ApJS, 154, 10
Fernandez Lorenzo M., Sulentic J., Verdes-Montenegro L., Ruiz J. E., Sabater J., Sánchez S., 2012, A&A, 540, 47
Fioc M., Rocca-Volmerange B., 1999, preprint (arXiv:astro-ph/9912179)
Fukugita M. et al., 2007, AJ, 134, 579
Goderya S. N., Lolling S. M., 2002, Ap&SS, 279, 377
Hales C. A., Murphy T., Curran J. R., Middelberg E., Gaensler B. M., Norris R. P., 2012, MNRAS, 425, 979
Hibbard J. E., Yun M. S., 1999, AJ, 118, 62
Hibbard J. E., van Gorkom J. H., Rupen M. P., Schiminovich D. S., 2001, in Hibbard J. E., Rupen M. P., van Gorkom J. H., eds, ASP Conf. Ser. Vol. 240, Gas and Galaxy Evolution. Astron. Soc. Pac., San Francisco, p. 659
Holwerda B. W., Pirzkal N., Cox T. J., de Blok W. J. G., Weniger J., Bouchard A., Blyth S.-L., van der Heyden K. J., 2011, MNRAS, 416, 2426
Holwerda B. W. et al., 2014, ApJ, 781, 12
Hoyos C. et al., 2012, MNRAS, 419, 2703
Huertas-Company M. et al., 2013, MNRAS, 428, 1715
Jog C., Combes F., 2009, Phys. Rep., 471, 75
Jogee S., Kenney J. D. P., Smith B. J., 1998, ApJ, 494, L185
Joye W. A., Mandel E., 2003, in Payne H. E., Jedrzejewski R. I., Hook R. N., eds, ASP Conf. Ser. Vol. 295, Astronomical Data Analysis Software and Systems XII. Astron. Soc. Pac., San Francisco, p. 489
Kennicutt R. C., Jr. et al., 2003, PASP, 115, 928
Kim T. et al., 2012, ApJ, 753, 43
Knapen J. H., Erroz-Ferrer S., Roa J., Bakos J., Cisternas M., Leaman R., Szymanek N., 2014, A&A, preprint (arXiv:1406.4107)
Kormendy J., 2012, in Falcon-Barroso J., Knapen J. H., eds, Secular Evolution of Galaxies. Cambridge Univ. Press, Cambridge, p. 1
Kormendy J., Bender R., 2012, ApJS, 198, 2
Lahav O., 1995, Astrophys. Lett., 31, 73
Lintott C. J. et al., 2008, MNRAS, 389, 1179
Lintott C. J. et al., 2011, MNRAS, 410, 166
Lotz J. M., Primack J., Madau P., 2004, AJ, 128, 163
Macció A. V., Moore B., Stadel J., 2006, ApJ, 636, L25
Malin D. F., Carter D., 1980, Nature, 285, 643
Martig M., Bournaud F., Teyssier R., Dekel A., 2009, ApJ, 707, 250
Martig M., Bournaud F., Croton D. J., Dekel A., Teyssier R., 2012, ApJ, 756, 26
Martínez-Delgado D., Peñarrubia J., Gabany R. J., Trujillo I., Majewski S. R., Pohlen M., 2008, ApJ, 689, 184
Martínez-Delgado D., Pohlen M., Gabany R. J., Majewski S. R., Peñarrubia J., Palma C., 2009, ApJ, 692, 955
Martínez-Delgado D. et al., 2010, AJ, 140, 962
Meidt S. et al., 2012a, ApJ, 744, 17
Meidt S. et al., 2012b, ApJ, 748, L30
Muñoz-Mateos J. C. et al., 2009, ApJ, 703, 1569
Muñoz-Mateos J. C. et al., 2014, ApJS, submitted
Nair P. B., Abraham R. G., 2010, ApJS, 186, 427
Ostriker E. C., Binney J. J., 1989, MNRAS, 237, 785
Reichard T. A., Heckman T. M., Rudnick G., Brinchmann J., Kauffmann G., 2008, ApJ, 677, 186
Reshetnikov V., Combes F., 1998, A&A, 337, 9
Reshetnikov V., Combes F., 1999, A&AS, 138, 101
Reshetnikov V. P., Faúndez-Abans M., Oliveira-Abans M., 2001, MNRAS, 322, 689
Rix H.-W., Zaritsky D., 1995, ApJ, 447, 82
Sales L., Lambas D. G., 2005, MNRAS, 356, 1045
Sánchez-Saavedra M. L., Battaner E., Guijarro A., López-Corradoira M., Castro-Rodríguez N., 2003, A&A, 399, 457
Sandage A., 2005, ARA&A, 43, 581
Scarlata C. et al., 2007, ApJS, 172, 406
Schweizer F., Seitzer P., 1988, ApJ, 328, 88
Schweizer F., Seitzer P., 1992, AJ, 104, 1039
Schweizer F., Whitmore B. C., Rubin V. C., 1983, AJ, 88, 909
Shamir L., 2009, MNRAS, 399, 1367
Sheth K. et al., 2010, PASP, 122, 1397
Storrie-Lombardi M. C., Lahav O., Sodre L., Jr, Storrie-Lombardi L. J., 1992, MNRAS, 259, 8
Tal T., van Dokkum P. G., Nelan J., Bezanson R., 2010, AJ, 138, 1417
Toomre A., Toomre J., 1972, ApJ, 178, 623
van Driel W. et al., 1995, AJ, 109, 942
Vorontsov-Velyaminov B. A., 1959 Atlas and Catalogue of Interacting Galaxies, Part I. Moscow Univ., Moscow
Vorontsov-Velyaminov B. A., 1977, A&AS, 28, 1
Wehner E. H., Gallagher J. S., Papaderos P., Fritze-von Alvensleben U., Westfall K. B., 2006, MNRAS, 371, 1047
Zaritsky D., Smith R., Frenk C., White S. D. M., 1993, ApJ, 405, 464
Zaritsky D. et al., 2013, ApJ, 772, 135

SUPPORTING INFORMATION

Additional Supporting Information may be found in the online version of this article:

Figure 1. Images of asymmetric outer discs in the S^{4}G sample.
Figure 2. Images of extensions in the S^{4}G sample.
Figure 3. Images of tidal tails in the S^{4}G sample.
Figure 5. Images of warps in the S^{4}G sample.
Figure 6. Images of interacting galaxies in the S^{4}G sample.
Figure 7. Images of merging galaxies in the S^{4}G sample.
Figure 15. Images of outer disc asymmetries in simulated galaxies.
Figure 16. Images of outer disc extensions in simulated galaxies (http://mnras.oxfordjournals.org/lookup/suppl/doi:10.1093/mnras/stu1642/-/DC1).

Please note: Oxford University Press is not responsible for the content or functionality of any supporting materials supplied by the authors. Any queries (other than missing material) should be directed to the corresponding author for the article.

[1]Spitzer *Science Center – Caltech, MS 314-6, Pasadena, CA 91125, USA*
[2]*Instituto de Astrofísica de Canarias, E-38205 La Laguna, Tenerife, Spain*
[3]*Departamento de Astrofísica, Universidad de La Laguna, E-38206 La Laguna, Spain*
[4]*National Radio Astronomy Observatory/NAASC, Charlottesville, 520 Edgemont Road, VA 22903, USA*
[5]*European Southern Observatory, Alonso de Cordova 3107, Vitacura, Casilla 19001, Santiago, Chile*
[6]*Astronomy Program, Department of Physics and Astronomy, Seoul National University, Seoul 151-742, Korea*
[7]*The Observatories of the Carnegie Institution of Washington, 813 Santa Barbara Street, Pasadena, CA 91101, USA*
[8]*Division of Astronomy, Department of Physics, University of Oulu, PO Box 3000, FI-90014 Oulu, Finland*

[9]*Finnish Centre of Astronomy with ESO (FINCA), University of Turku, Väisäläntie 20, FI-21500 Piikkiö, Finland*
[10]*Max-Planck Institut für Astronomie, Königstuhl 17, D-69117 Heidelberg, Germany*
[11]*Leiden Observatory, Leiden University, PO Box 9513, NL-2300 RA Leiden, the Netherlands*
[12]*Aix Marseille Université, CNRS, LAM (Laboratoire d'Astrophysique de Marseille), UMR 7326, F-13388 Marseille 13, France*
[13]*Department of Physics, University of Helsinki, Gustaf Hällströmin katu 2a, FI-00014 Helsinki, Finland*
[14]*Departamento de Astrofísica y CC. de la Atmósfera, Universidad Complutense de Madrid, Avda. de la Complutense s/n, E-28040 Madrid, Spain*
[15]*MMTO, University of Arizona, 933 N. Cherry Avenue, Tucson, AZ 85721, USA*
[16]*Universidade Federal do Rio de Janeiro, Observatório do Valongo, Ladeira do Pedro Antônio 43, CEP 20080-090 Rio de Janeiro, Brazil*
[17]*Florida Institute of Technology, Melbourne, FL 32901, USA*
[18]*Space Telescope Science Institute, 3700 San Martin Drive, Baltimore, MD 21218, USA*
[19]*California Institute of Technology, 1200 East California Boulevard, Pasadena, CA 91125, USA*
[20]*Department of Physics and Astronomy, University of Alabama, Box 870324, Tuscaloosa, AL 35487, USA*
[21]*IBM Research Division, T. J. Watson Research Center, 1101 Kitchawan Road, Yorktown Heights, NY 10598, USA*
[22]*Department of Physics and Astronomy, Vassar College, Poughkeepsie, NY 12604, USA*
[23]*Kavli Institute for Astronomy and Astrophysics, Peking University, Beijing 100871, China*
[24]*Steward Observatory, University of Arizona, 933 North Cherry Avenue, Tucson, AZ 85721, USA*

This paper has been typeset from a TEX/LATEX file prepared by the author.